A Comprehensive Mechanism for Methanol Oxidation

TIMOTHY J. HELD,* FREDERICK L. DRYER

Department of Mechanical and Aerospace Engineering, Princeton University, Princeton, New Jersey 08544-5263

Received 24 February 1997; accepted 8 May 1998

ABSTRACT: A comprehensive detailed chemical kinetic mechanism for methanol oxidation has been developed and validated against multiple experimental data sets. The data are from static-reactor, flow-reactor, shock-tube, and laminar-flame experiments, and cover conditions of temperature from 633–2050 K, pressure from 0.26–20 atm, and equivalence ratio from 0.05–2.6. Methanol oxidation is found to be highly sensitive to the kinetics of the hydroperoxyl radical through a chain-branching reaction sequence involving hydrogen peroxide at low temperatures, and a chain-terminating path at high temperatures. The sensitivity persists at unusually high temperatures due to the fast reaction of $CH_2OH + O_2 = CH_2O + HO_2$ compared to $CH_2OH + M = CH_2O + H + M$. The branching ratio of $CH_3OH + OH = CH_2OH/CH_3O + H_2O$ was found to be a more important parameter under the higher temperature conditions, due to the rate-controlling nature of the branching reaction of the H-atom formed through CH_3O thermal decomposition. © 1998 John Wiley & Sons, Inc. Int J Chem Kinet 30: 805–830, 1998

INTRODUCTION

Detailed chemical kinetic mechanisms can be useful engineering tools, which permit exploration of the microscopic chemical processes that underlie and sometimes control the macroscopic physical processes, such as flame speed or autoignition time. The mechanisms are systems of many elementary reactions, with rate constants determined, where possible, by fundamental kinetic experiments or theoretical treatment. The examination of the contribution of the elementary reactions within the context of the larger system aids in identification of rate constants or reaction channels that warrant further investigation by fundamental kineticists.

Detailed mechanisms are often developed in response to and validated against a single set of experimental measurements. As a result, the range of applicability of the mechanism, as defined primarily by temperature, pressure, and equivalence ratio, is limited to that covered by the data set. The term "comprehensive" implies that the range of validity of the mechanism has been extended to the maximum practical extent by comparison to multiple experimental data sets. The creation of such mechanisms has additional utility. Many combustion processes occur over a wide range of conditions (An example is the autoignition process in spark-ignition engines. The fuel/air charge enters the cylinder at near-ambient conditions, and in a transient process, is compressed to 10–40 atm, and an unburned gas temperature of 1000–1200 K). A comprehensive mechanism may be used to not only identify important reactions, but also the controlling chemical regimes during the transient process.

In the present work, a detailed kinetic mechanism,

* *Present address:* GE Aircraft Engines, One Neumann Way, Cincinnati, OH 45215-1915.

Correspondence to: F. L. Dryer (E-mail:fldryer@princeton.edu)

Contract grant Sponsor: National Science Foundation Fellowship

Contract grant Sponsor: U.S. Department of Energy, Chemical Sciences Division, Office of Basic Energy Sciences

Contract grant number: DE-FG02-86ER-13503

 CCC 0538-8066/98/110805-26

initially developed in comparison to low and intermediate temperature (< 1100 K) flow reactor data, is extended by comparison to shock-tube, flame-speed, and static-reactor data. Reaction path and sensitivity analysis is used to identify controlling reaction channels and rate constants, and to indicate several reactions that require additional study.

PREVIOUS MODELING STUDIES

Westbrook and Dryer

The first comprehensive detailed kinetic model of methanol oxidation was developed by Westbrook and Dryer [1]. Inclusion of reaction paths that were important at both high and intermediate temperatures produced successful reproduction of flow-reactor and shock-tube data. Using a simplified diffusion model, the stoichiometric laminar flame speed of a premixed methanol/air mixture was calculated to be 44 ± 2 cm/s at one atmosphere, 298 K initial conditions.

The work was hampered by a lack of elementary rate constant and reaction path information. Many important rate constants, including those for methanol and hydroxymethyl (CH_2OH) thermal decomposition, and H and OH abstraction reactions, were estimated in the context of the detailed modeling. The methoxy radical (CH_3O) was neglected in the mechanism. Considerable importance was placed upon the dehydration reaction

$$CH_3OH + OH = CH_3 + H_2O$$

as a source of methane and C_2 hydrocarbons. Later work [2] has indicated that this reaction route is negligible, and other sources are sufficient to account for experimental methane and C_2 species measurements. The effects of pressure-dependent reactions were not included in this early modeling effort.

Norton and Dryer

Oxidation Mechanism: In an effort to resolve several difficulties with the Westbrook/Dryer [1] mechanism, Norton and Dryer updated the model using more current rate constants and a consistent set of thermochemical parameters [3]. In a few instances, different product paths were proposed based on more recent work. The updated mechanism was compared to a new set of atmospheric-pressure flow-reactor data [4], encompassing the temperature range of 1025–1090 K and equivalence ratios from 0.6–1.6. Improved agreement with the flow-reactor data was attained, and the importance of the hydroperoxyl radical (HO_2) to methanol oxidation kinetics was identified. No attempt was made to recalculate the full experimental basis set from the original reference [1].

Comprehensive Pyrolysis Mechanism: The same authors expanded upon their previous work to develop a comprehensive model for methanol pyrolysis [2]. Although not an oxidation mechanism, many of the important reaction paths in high-temperature oxidation are identical to those found in pyrolysis studies as well. The mechanism was compared successfully to static-reactor, flow-reactor, and shock-tube data.

Egolfopoulos, Du, and Law

A more recent attempt [5] at creating a comprehensive methanol oxidation mechanism was based primarily upon premixed laminar flame-speed measurements over a range of initial temperatures and pressures. Excellent agreement was attained for both the laminar flame speed and atmospheric-pressure flow-reactor data set [4]. The agreement with Bowman's shock-tube ignition delay measurements [6] was less satisfactory, and only a small subset of the data were reported. Laminar-flame-species profiles were compared to data of Vandooren and Van Tiggelen [7,8], Pauwels et al. [9], and Bradley [10]. Although the calculation technique was not specified, it is apparent that the species profiles were forced to match the data point closest to the burner face. It is therefore difficult to judge the accuracy of the premixed flame profile calculations.

Unfortunately, the products of a $CH_3 + OH$ reaction were erroneously assigned as $CH_2OH + H$ rather than $CH_3O + H$ [11]. The resulting reverse reaction rate coefficient is higher than collisional, and significantly affects the calculated results. With the product channel correctly specified, the mechanism calculates flame speeds in substantial disagreement with the authors' experimental measurements. The error also overemphasizes the relative importance of C_2 chemistry due to the higher CH_3 production rate and alters the sensitivity of the calculations to the $CH_3OH + OH = CH_2OH/CH_3O + H_2O$ branching ratio, as discussed further below.

Grotheer

Although not described as a comprehensive mechanism, the model of Grotheer et al., [12,13] has been applied to both premixed laminar flame speed calculations and to autoignition in a spark-ignition engine [14]. The published comparison of flame speed to experimental data is excellent. Gradient sensitivity co-

efficients for flame speed identify a number of important reactions, including $HO_2 + H =$ products and hydroxymethyl decomposition.

The authors also identified the branching ratio between $CH_3OH + OH = CH_2OH/CH_3O + H_2O$ (defined as k_{CH_2OH}/k_{total}) as an important parameter in calculating flame speeds. The value chosen to give optimal agreement with the measurements is 0.85. Several independent experimental and theoretical studies of the OH abstraction reaction, indicate an increasing contribution of the methoxy radical path with increasing temperature, approaching a value of the branching ratio of 0.5 above 865 K. Substitution of the lower branching ratio into the baseline mechanism would result in a significant increase in the calculated laminar flame speeds.

DETAILED MECHANISM DEVELOPMENT

Mechanism Development

The development of a detailed kinetic model is a hierarchical procedure. The basis for any hydrocarbon oxidation is the subset of reactions involving hydrogen, oxygen, and their associated intermediates and products. These include H- and O-atoms, hydroxyl (OH) and hydroperoxyl (HO_2) radicals, and hydrogen peroxide (H_2O_2). and water. This submechanism determines to a large extent the characteristics of the radical pool responsible for chain propagation, termination, and branching.

The oxidation of carbon-containing species follows a basic series of steps, beginning with initiation reactions, followed by radical attack on the fuel, production of (generally) smaller intermediates, and finally a chain of aldehyde $\rightarrow$ CO $\rightarrow$ CO_2 steps [15]. Taken in inverse order, these steps form the basic reaction hierarchy in a detailed kinetic mechanism.

This section describes the procedures and sources used in compiling the detailed models of this study. Although attention is preferentially focused upon reactions of the most significance to the mechanism, discussion of the relative importance of individual reactions appears in the following sections where relevant.

$CO/H_2/O_2$

The carbon monoxide/hydrogen/oxygen reaction system used in this study is taken primarily from the mechanism of Yetter et al. [16], which has been recently modified to reflect high-pressure studies of Kim et al. [17,18]. This submechanism was verified against a series of flow-reactor, static-reactor, and shock-tube experiments, and is well established as providing an accurate depiction of hydrogen and carbon monoxide oxidation over a wide range of conditions.

CH_2O

Formaldehyde oxidation kinetics are of great importance to the oxidation of larger hydrocarbon and oxygenated hydrocarbon species. Under most circumstances, nearly all of the carbon in these species is oxidized through a route involving formaldehyde. Methanol oxidation is not an exception to this generalization. Thus, accurate modeling of methanol oxidation requires significant attention to the details of the formaldehyde oxidation mechanism as well.

The difficulties involved in generating formaldehyde have resulted in a relatively sparse experimental data set for mechanism validation [19]. The comprehensive modeling effort of Hochgreb and Dryer [20] encompassed the full range of available data, including shock-tube, flow-reactor, and static-reactor data. For the present modeling study, the CH_2O submechanism was modified as described in an earlier article [21]. The rate constants of $CH_2O + H$ and $CH_2O + OH$ were reduced from their high values in the earlier work. These changes were necessary to reproduce peak formaldehyde yields in the flow reactor experiments [22]. The new rate constants for these reactions allowed accurate calculation of the relative formaldehyde and methanol destruction rates in flow-reactor experiments on the oxidation and pyrolysis of mixtures of these two species. Recalculation of the data set used in the original mechanism development [20] showed little change in the calculated species profiles, with the exception of the oxidative pyrolysis flow-reactor experiments. However, the presence of an uncontrolled trace contamination of oxygen in these experiments casts uncertainty upon their accuracy. Considering this uncertainty, the alteration of the calculated formaldehyde consumption rate is within the error limit of the experiments.

CH_3OH

The methanol submechanism requires addition of the following species: methanol (CH_3OH), hydroxymethyl (CH_2OH), and methoxy (CH_3O). The high-pressure flow-reactor experiments indicated the presence of formic acid (HCOOH) and 1,2-ethanediol (ethylene glycol, HOC_2H_4OH) as minor intermediates. For the present work, tentative formation mechanisms for these species are described below. The two methanol mechanisms of Norton and Dryer provided the initial basis for the present methanol submechanism.

A number of rate constants were changed from the original mechanisms to reflect more recent rate constant measurements. The details of the most significant portions of the mechanism are discussed below.

Initiation/Decomposition: Although the rate constants of initiation reactions are seldom important under flow-reactor, static-reactor, or laminar-flame conditions, they may play a more significant role in shock-tube studies. At least four different decomposition reactions are possible:

$$\begin{aligned} CH_3OH + M &= CH_3 + OH & \Delta H_r &= 92.2 \text{ kcal/mol} \\ &= CH_2OH + H & & 98.0 \text{ kcal/mol} \\ &= CH_3O + H & & 104.1 \text{ kcal/mol} \\ &= {}^1CH_2 + H_2O & & 91.8 \text{ kcal/mol} \end{aligned}$$

The first reaction predominates, accounting for 75% to 90% of the total decomposition rate in various studies [23–25]. The methoxy radical channel is thermodynamically unfavorable. The hydroxymethyl channel is usually assumed to account for the remainder of the initiation rate, although the singlet methylene channel is an interesting alternative proposed by Dombrowsky et al. [23]. As yet there is no direct evidence to support this channel, but it could be considered in future studies.

For the present model, a Troe fit for the $CH_3 + OH$ channel was generated based on the falloff parameters of Tsang [26]. For simplicity, the hydroxymethyl channel is assigned a rate of 10% of the primary channel. A more accurate expression should take into account the higher activation energy expected with the more endothermic reaction path; however, the calculations are insensitive to the rate constant of this reaction.

OH Abstraction: The abstraction reactions of OH are the predominant fuel consumption routes in the methanol mechanism. The abstraction may occur at either the methyl or hydroxyl group, forming $CH_2OH + H_2O$ (83) or $CH_3O + H_2O$ (84), respectively. Except at the highest temperatures, the two species react by considerably different mechanisms

$$CH_2OH + O_2 = CH_2O + HO_2 \qquad (70)$$

$$CH_3O + M = CH_2O + H + M \qquad (42)$$

It is therefore important to maintain a distinction between the two CH_3O isomers.

Two recent studies reported overall rates for the reaction of methanol with OH. Hess and Tully [27] obtained an expression for $k_{83} + k_{84} = 3.54 \times 10^4 T^{2.6} \exp(883/RT)$ over the temperature range 293–803 K*. Isotopic substitution allowed an estimate of the "branching ratio," defined as $k_{83}/(k_{83} + k_{84})$, that increased from a small value to 0.5 at their highest temperature. More recently, Bott and Cohen [28] obtained a value for $k_{83} + k_{84}$ of 5.2×10^{12} at 1200 K, in excellent agreement with the value of 5.1×10^{12} obtained from the previous expression. Their calculated site specific expressions yield a branching ratio that increases from 0.39 at 1000 K to 0.51 at 2000 K. The present mechanism uses the expression of Bott and Cohen.

Reaction with H: Methanol may react with hydrogen atoms by abstraction from either site, or by dehydration, forming methyl and water. The latter reaction was suggested as a significant source of methyl radicals [1], although subsequent studies [2] have failed to detect evidence of this channel. The present model does not include this reaction. Its inclusion at the rate constant suggested by Norton [3] has no discernible effect on the overall kinetics.

The abstraction reaction consumes a significant fraction of the methanol, particularly under fuel rich conditions. The product channel yielding hydroxymethyl is 6.1 kcal/mol exothermic, while the methoxy channel is almost thermoneutral. Consistent with the pyrolysis study of Norton and Dryer [2], the rate constant of Warnatz [29] was applied with a 20% contribution by the methoxy radical path.

CH_3O/CH_2OH Isomerization: A possible isomerization reaction between CH_3O and CH_2OH was first suggested as a loss mechanism for CH_3O in a fundamental kinetics experiment [30]. Because thermodynamic equilibrium strongly favors hydroxymethyl, the isomerization primarily converts methoxy to hydroxymethyl. Because it eliminates the H-atom produced by methoxy decomposition, the isomerization reaction could be very important if it occurs at a rate comparable to the decomposition rate. Theoretical and thermochemical estimates of the isomerization rate constant [31–33] consistently place its value at or below about 10% of that for methoxy decomposition. Experimental work [34] also suggests that the upper limit for the isomerization reaction is 10% of the decomposition rate. At this upper limit, the isomerization reaction does not significantly affect the results of the detailed model. Since no direct evidence exists to support this reaction path, the present mechanism does not include it.

Minor Species Formation: Infrared spectra collected during the VPFR experiments indicated the presence of detectable amounts of formic acid as an intermediate species (approximately 50 ppm with 4000 ppm

* mol-cm^3-cal-s units are used unless noted.

initial methanol). A postulated formation mechanism is a combination reaction between hydroxymethyl and hydroperoxyl radicals, followed by decomposition or rearrangement and decomposition:

$$CH_2OH + HO_2 = CH_2(OOH)OH$$

$$CH_2(OOH)OH = CH_2(O)OH + OH$$

-or-

$$CH_2(OOH)OH = HCOOH + H_2O$$

$$CH_2(O)OH = HCOOH + H$$

Spangenberg et al. [35] originally postulated the dehydration route, which involves a fairly highly strained transition state. The decomposition route seems more likely, but there is no direct evidence to support one path over the other. The present mechanism includes both reactions with estimated rate coefficients of 3.0×10^{13} cm^3/mol-s. The variation of formic acid mole fraction with equivalence ratio is not well reproduced, and thus this mechanism can only be considered tentative, at best.

In the most fuel-rich high-pressure flow-reactor experiments, a spectral feature identified as 1,2-ethanediol (ethylene glycol) was detected after the oxygen had been completely consumed [21,22]. Clearly, this species is a product of hydroxymethyl (CH2OH) dimerization. Although the quality of the spectrum was insufficient to permit its quantification, the possibility that 1,2-ethanediol formation is an important radical termination path for fuel-rich conditions led to the inclusion of this reaction in the mechanism. However, its impact on the overall predictions of the mechanism is negligible.

C_2 Species: Because small amounts of methyl radicals are created during the oxidation and pyrolysis of methanol, C_2 or larger hydrocarbon species may be formed by their recombination. Egolfopoulos et al. [5] reported significant effects of the inclusion of a detailed C_2 submechanism on their calculated laminar flame speeds. Because of the incorrectly high-rate constant for $CH_2OH + H = CH_3 + OH$ used in their mechanism [11,13], it is likely that this conclusion is influenced by an erroneously high CH_3 production rate. In the present work, a simple C_2 mechanism was assembled primarily from the compilation of Tsang and Hampson [36] for purposes of testing the influence of higher carbon number kinetics on methanol oxidation. Under all cases simulated, no influence of C_2 chemistry could be detected in any of the calculated species profiles, overall reaction rates, ignition delays or premixed flame speeds.

Summary: The cumulative mechanism used for comparison to the methanol experiments appears in Table I, with the forward rate coefficients and references. The reverse reaction rates are calculated by detailed balance and thermodynamic parameters, listed in Table II. Most of these data are from the Sandia thermodynamic database [37]. The enthalpy of formation for CH_2OH has been changed to reflect the recent measurements of Seetula and Gutman [38].

Solution Technique

Six different types of experiments were simulated in this study, static reactors, flow reactors, shock tubes, premixed flames extrapolated to the freely-propagating, unstretched condition, and burner-stabilized flat premixed flames. The Chemkin-II package [39] was used for the simulations. The fundamental modeling assumptions are summarized as follows.

Static Reactor: Constant volume, spatially homogeneous. The assumption of a spatially homogeneous mixture requires that the reaction time is much longer than the characteristic thermal and mass diffusion times to the reactor walls. The implications of these characteristics of static reactor experiments are discussed below.

Flow Reactor: Constant pressure, adiabatic, zero-dimensional. The constant pressure assumption is essentially a low Mach number assumption. Adiabaticity is approximated in the experiments through the use of preheated reactor tube walls and a short length to diameter ratio in the reactor tube. Zero-dimensionality is valid in the case of negligible axial and radial diffusion. Radial diffusion is held to a minimum, again by limiting the experiment to L/D values such that the flow is essentially an entry-region flow, where the developing boundary layers do not interact strongly with a radially uniform core flow. Finally, axial diffusion is negligible where the characteristic diffusion length is much greater than the convective length. Although this assumption is reasonably valid over much of the reaction zone, it breaks down in regions of high concentration gradients, such as in the rapid transition in the oxidation rate of CO accompanying the depletion of hydrocarbon species in Figure 12.

The finite-rate mixing of fuel and oxidizer, recirculation zones near the mixing region, and residual effects of axial diffusion in this region all result in uncertainty in specification of an absolute “zero time” for flow reactor experiments. Modeling simulation of these effects using stirred reactor-plug flow coupled models has shown that they all serve to translate the calculated species and temperature profiles along the time axis toward the origin. Furthermore, the initial perturbations of the system are quickly relaxed and result in no historical effects downstream of this re-

Table I Methanol Oxidation Reaction Mechanism

	Reaction		A (cm-mol-s)	n	E_a (cal/mol)	Ref.
H_2/O_2						
1	$H + O_2 = O + OH$		1.92×10^{14}	0	16439	[74]
2	$O + H_2 = H + OH$		5.08×10^{04}	2.67	6290	[75]
3	$H_2 + OH = H_2O + H$		2.16×10^{08}	1.51	3430	[78]
4	$O + H_2O = OH + OH$		2.97×10^{06}	2.02	13400	[77]
5	$H_2 + M = H + H + M$		4.58×10^{19}	−1.40	104380	[78][a]
	$H_2 + Ar = H + H + Ar$		5.84×10^{18}	−1.10	104380	[78]
6	$O + O + M = O_2 + M$		6.17×10^{15}	−0.50	0	[79][a]
	$O + O + Ar = O_2 + Ar$		1.89×10^{13}	0	−1788	[79]
7	$O + H + M = OH + M$		4.71×10^{18}	−1.00	0	[36][b]
8	$H + OH + M = H_2O + M$		2.21×10^{22}	−2.00	0	[80][c]
9	$H + O_2(+M) = HO_2(+M)$	k_∞	4.52×10^{13}	0	0	[81][a,d]
		k_0	6.70×10^{19}	−1.42	0	[82]
	$H + O_2(+Ar) = HO_2(+Ar)$	k_∞	4.52×10^{13}	0	0	[81]
		k_0	6.17×10^{17}	0.80	0	[83]
			$F_{cent} = 0.5$			
10	$HO_2 + H = H_2 + O_2$		6.63×10^{13}	0	2130	[36]
11	$HO_2 + H = OH + OH$		1.69×10^{14}	0	874	[36]
12	$HO_2 + O = O_2 + OH$		1.81×10^{13}	0	−397	[36]
13	$HO_2 + OH = H_2O + O_2$		1.90×10^{16}	−1.00	0	[18]
14	$HO_2 + HO_2 = H_2O_2 + O_2$		4.20×10^{14}	0	11982	[84]
		+[e]	1.30×10^{11}	0	−1629	
15	$H_2O_2(+M) = OH + OH(+M)$	k_∞	2.95×10^{14}	0	48430	[85][a]
		k_0	1.20×10^{17}	0	45500	[29]
			$F_{cent} = 0.5$			
	$H_2O_2(+Ar) = OH + OH(+Ar)$	k_∞	2.95×10^{14}	0	48430	[85]
		k_0	1.90×10^{16}	0	43000	[85]
			$F_{cent} = 0.5$			
16	$H_2O_2 + H = H_2O + OH$		1.00×10^{13}	0	3590	[29]
17	$H_2O_2 + H = HO_2 + H_2$		4.82×10^{13}	0	7950	[36]
18	$H_2O_2 + O = OH + HO_2$		9.55×10^{06}	2.00	3970	[36]
19	$H_2O_2 + OH = HO_2 + H_2O$		1.00×10^{12}	0	0	[86]
		+	5.80×10^{14}	0	9557	
CO						
20	$CO + O + M = CO_2 + M$		2.51×10^{13}	0	−4540	[29][f]
21	$CO + O_2 = CO_2 + O$		2.53×10^{12}	0	47700	[36]
22	$CO + OH = CO_2 + H$		1.50×10^{07}	1.30	−765	[87]
23	$CO + HO_2 = CO_2 + OH$		6.02×10^{13}	0	23000	[88]
HCO/CH_2O						
24	$HCO + M = H + CO + M$		1.86×10^{17}	−1.00	17000	[89][b]
25	$HCO + O_2 = CO + HO_2$		7.58×10^{12}	0	410	[90]
26	$HCO + H = CO + H_2$		7.23×10^{13}	0	0	[91]
27	$HCO + O = CO + OH$		3.02×10^{13}	0	0	[36]
28	$HCO + O = CO_2 + H$		3.00×10^{13}	0	0	[36]
29	$HCO + OH = CO + H_2O$		3.02×10^{13}	0	0	[36]
30	$HCO + HO_2 = CO_2 + OH + H$		3.00×10^{13}	0	0	[36]
31	$HCO + CH_3 = CO + CH_4$		1.20×10^{14}	0	0	[36]
32	$HCO + HCO = CH_2O + CO$		1.80×10^{13}	0	0	[36]
33	$HCO + HCO = H_2 + CO + CO$		3.00×10^{12}	0	0	[36]
34	$CH_2O + M = HCO + H + M$		4.00×10^{23}	−1.66	91470	[20]
35	$CH_2O + M = CO + H_2 + M$		8.25×10^{15}	0	69540	[67]
36	$CH_2O + H = HCO + H_2$		1.14×10^{08}	1.66	1834	[21]

(Continued)

Table I (Continued)

	Reaction		A (cm-mol-s)	n	E_a (cal/mol)	Ref.
37	$CH_2O + O = HCO + OH$		1.81×10^{13}	0	3080	[92]
38	$CH_2O + OH = HCO + H_2O$		4.80×10^{09}	1.18	−447	[21]
39	$CH_2O + O_2 = HCO + HO_2$		2.00×10^{13}	0	39000	[93]
40	$CH_2O + HO_2 = HCO + H_2O_2$		1.50×10^{13}	0	15200	[20]
41	$CH_2O + CH_3 = HCO + CH_4$		5.54×10^{03}	2.81	5862	[36]
CH_3O						
42	$CH_3O + M = CH_2O + H + M$		8.30×10^{17}	−1.20	15500	[94]
43	$CH_3O + H = CH_2O + H_2$		2.00×10^{13}	0	0	[65]
44	$CH_3O + H = CH_3 + OH$		3.20×10^{13}	0	0	[95]
45	$CH_3O + O = CH_2O + OH$		6.00×10^{12}	0	0	[36]
46	$CH_3O + OH = CH_2O + H_2O$		1.80×10^{13}	0	0	[36]
47	$CH_3O + O_2 = CH_2O + HO_2$		9.03×10^{13}	0	11980	[96]
		+	2.20×10^{10}	0	1748	
48	$CH_3O + HO_2 = CH_2O + H_2O_2$		3.00×10^{11}	0	0	[36]
49	$CH_3O + CO = CH_3 + CO_2$		1.60×10^{13}	0	11800	[97]
50	$CH_3O + HCO = CH_3OH + CO$		9.00×10^{13}	0	0	[36]
51	$CH_3O + CH_3O = CH_3OH + CH_2O$		6.00×10^{13}	0	0	[36]
CH_3/CH_4						
52	$CH_3 + O = CH_2O + H$		8.43×10^{13}	0	0	[98]
53	$CH_3 + O_2 = CH_3O + O$		1.99×10^{18}	−1.57	29230	[36]
54	$CH_3 + HO_2 = CH_3O + OH$		2.00×10^{13}	0	1076	[99]
55	$CH_3 + CH_3(+M) = C_2H_6(+M)$	k_∞	9.03×10^{16}	−1.18	654	[100]
		k_0	3.18×10^{41}	−7.03	2762	
			$F_{cent} = (1 - 0.619)\, e^{(-T/73.2\ \mathrm{K})} + 0.619\, e^{(-T/1180\ \mathrm{K})}$			
56	$CH_4(+M) = CH_3 + H(+M)$	k_∞	3.70×10^{15}	0	103800	[101]
		k_0	7.21×10^{30}	−3.49	105900	
57	$CH_4 + H = CH_3 + H_2$		5.47×10^{07}	1.97	11210	[102]
58	$CH_4 + O = CH_3 + OH$		6.93×10^{08}	1.56	8484	[103]
59	$CH_4 + OH = CH_3 + H_2O$		5.72×10^{06}	1.96	2639	[104]
60	$CH_4 + O_2 = CH_4 + HO_2$		4.00×10^{13}	0	56910	[105]
61	$CH_4 + HO_2 = CH_3 + H_2O_2$		1.81×10^{11}	0	18580	[36]
HCOOH						
62	$HCOOH + M = CO + H_2O + M$		2.09×10^{14}	0	40400	[106]
63	$HCOOH + M = CO_2 + H_2 + M$		1.35×10^{15}	0	60600	[106]
64	$HCOOH + OH = H_2O + CO_2 + H$		3.00×10^{11}	0	0	[107]
CH_2OH						
65	$CH_2OH(+M) = CH_2O + H(+M)$	k_∞	2.80×10^{14}	−0.73	32820	[26][g,h]
		k_0	6.01×10^{33}	−5.39	36200	
			$F_{cent} = (1 - 0.96)\, e^{(-T/67.6\ \mathrm{K})} + 0.96\, e^{(-T/1855\ \mathrm{K})} + e^{(-7543/T)}$			
66	$CH_2OH + H = CH_2O + H_2$		6.00×10^{12}	0	0	[26]
67	$CH_2OH + H = CH_3 + OH$		9.63×10^{13}	0	0	[36]
68	$CH_2OH + O = CH_2O + OH$		4.20×10^{13}	0	0	[26]
69	$CH_2OH + OH = CH_2O + H_2O$		2.40×10^{13}	0	0	[26]
70	$CH_2OH + O_2 = CH_2O + HO_2$		2.41×10^{14}	0	5017	[108]
		+	1.51×10^{15}	−1.00	0	
71	$CH_2OH + HO_2 = CH_2O + H_2O_2$		1.20×10^{13}	0	0	[26]
72	$CH_2OH + HO_2 = HCOOH + OH + H$		2.00×10^{13}	0	0	[i]
73	$CH_2OH + HCO = CH_3OH + CO$		1.20×10^{14}	0	0	[26]
74	$CH_2OH + HCO = CH_2O + CH_2O$		1.80×10^{14}	0	0	[26]
75	$2CH_2OH = HOC_2H_4OH$		6.00×10^{12}	0	0	[26]
76	$2CH_2OH = CH_3OH + CH_2O$		3.00×10^{12}	0	0	[26]
77	$CH_2OH + CH_3O = CH_3OH + CH_2O$		2.40×10^{13}	0	0	[26]

(Continued)

Table I (Continued)

	Reaction		A (cm-mol-s)	n	E_a (cal/mol)	Ref.
CH_3OH						
78	$CH_3OH(+M) = CH_3 + OH(+M)$	k_∞	1.90×10^{16}	0	91730	[26][g,j]
		k_0	2.95×10^{44}	−7.35	95460	
			$F_{cent} = (1 - 0.414)\, e^{(-T/279\ K)} + 0.414\, e^{(-T/5459\ K)}$			
79	$CH_3OH(+M) = CH_2OH + H(+M)$	k_∞	2.69×10^{16}	−0.08	98940	[26][g,k]
		k_0	2.34×10^{40}	−6.33	103100	
			$F_{cent} = (1 - 0.773)\, e^{(-T/693\ K)} + 0.773\, e^{(-T/5333\ K)}$			
80	$CH_3OH + H = CH_2OH + H_2$		1.44×10^{13}	0	6095	[21]
81	$CH_3OH + H = CH_3O + H_2$		3.60×10^{12}	0	6095	[21]
82	$CH_3OH + O = CH_2OH + OH$		3.88×10^{05}	2.50	3080	[26]
83	$CH_3OH + OH = CH_2OH + H_2O$		7.10×10^{06}	1.80	−596	[28]
84	$CH_3OH + OH = CH_3O + H_2O$		1.00×10^{06}	2.10	496.7	[28]
85	$CH_3OH + O_2 = CH_2OH + HO_2$		2.05×10^{13}	0	44900	[26]
86	$CH_3OH + HCO = CH_2OH + CH_2O$		9.63×10^{03}	2.90	13110	[26]
87	$CH_3OH + HO_2 = CH_2OH + H_2O_2$		3.98×10^{13}	0	19400	[44]
88	$CH_3OH + CH_3 = CH_2OH + CH_4$		3.19×10^{01}	3.17	7172	[26]
89	$CH_3OH + CH_3O = CH_3OH + CH_2OH$		3.00×10^{11}	0	4060	[26]

[a] Enhanced third body efficiencies (relative to N_2): $\eta_{H_2} = 2.5$; $\eta_{H_2O} = 12$; $\eta_{CO} = 1.9$; $\eta_{CO_2} = 3.8$; and $\eta_{Ar} = 0$. Unless otherwise specified, all species are assumed to have a third body efficiency of 1.0.

[b] Enhanced third body efficiencies (relative to N_2): $\eta_{H_2} = 2.5$; $\eta_{H_2O} = 12$; $\eta_{CO} = 1.9$; $\eta_{CO_2} = 3.8$; and $\eta_{Ar} = 0.75$.

[c] Enhanced third body efficiencies (relative to N_2): $\eta_{H_2} = 2.5$; $\eta_{H_2O} = 6.3$; $\eta_{CO} = 1.9$; $\eta_{CO_2} = 3.8$; and $\eta_{Ar} = 0.38$.

[d] Pressure dependent reaction $-k_0$ and k_∞ refer to low- and high-pressure limits, respectively. Reactions with specified F_{cent} parameters use the Troe form, all others use the Lindemann expression [39].

[e] Indicates two or more Arrhenius expressions are summed for the net rate coefficient.

[f] Enhanced third body efficiencies (relative to N_2): $\eta_{H_2} = 2.5$; $\eta_{H_2O} = 12$; $\eta_{CO} = 1.9$; $\eta_{CO_2} = 3.8$; and $\eta_{Ar} = 0.87$.

[g] Troe fit to tabular falloff data of Tsang [26], using full available range of temperature and molar concentration. Expressions are for nitrogen as a collider, using $<\Delta E>_{down} = 500\ cm^{-1}$.

[h] Maximum fit error ±15%.

[i] Tsang's [36] rate constant for $CH_3CO + HO_2 = CO_2 + CH_3 + OH$. Assumes recombination followed by rapid decomposition to products.

[j] Maximum fit error +25/−30%.

[k] Maximum fit error: +35/−30% for $k > 10^{13}\ s^{-1}$.

gion, other than shifting the entire reaction profiles (without perturbations) with respect to the "zero time." When the calculated profiles are artificially temporally aligned at an arbitrary reference point within the downstream reaction zone where methanol disappearance is observed, the calculations and experimental profiles overlay one another nearly perfectly. Thus, in comparing calculations with experimental data, the time axis of the data is effectively "translated" to achieve a minimum RMS error with the calculated fuel decay profile. The magnitude of the required shift is noted in the figure captions. Time shifting and the results achieved by the above approach are entirely consistent with the assumption (noted above) that within the range of extents of reaction to be compared with the calculation, axial diffusion time scales are much longer than kinetic and convective time scales. Mathematically, the solution of the conservation equations then becomes an initial value problem, and any single matching point between the experiment and computation is equivalent (Computationally, calculations can be marched upstream or downstream of the matching point without concern).

Shock Tubes: The thermal environment in the post-shock region can be safely assumed to be adiabatic. Also, the short reaction time scales relative to diffusive times permits the zero-dimensional approximation. The treatment of the free boundary of the reaction zone is open to some debate. A limiting case, frequently applied, assumes a constant-volume (density) boundary, which implies that the bulk expansion of the fluid due to temperature rise and average molecular weight change overwhelms the inertial effects of the surrounding fluid. However, the situation is rarely as clear-cut as the simplified model would indicate. Short of solving the one-dimensional momentum equation, the best that can be assumed is that reality lies between the limiting cases of constant density and constant

Table II Thermodynamic Data for Methanol Mechanism

Species	$\Delta H_{f,298}$	S_{298}	$c_{p,300}$	c_{p500}	$c_{p,800}$	$c_{p,1000}$	$c_{p,1500}$	$c_{p,2000}$	
H	52.09	27.39	4.97	4.97	4.97	4.97	4.97	4.97	
O	59.55	38.46	5.23	5.08	5.02	5.00	4.98	4.98	
OH	9.32	43.88	7.15	7.07	7.13	7.33	7.87	8.28	
H_2	0.00	31.21	6.90	7.00	7.07	7.21	7.73	8.18	
O_2	0.00	49.00	7.01	7.44	8.07	8.35	8.72	9.03	
H_2O	−57.80	45.10	8.00	8.44	9.22	9.87	11.26	12.22	
HO_2	3.50	54.43	8.36	9.48	10.75	11.37	12.34	12.90	
H_2O_2	−32.53	55.65	10.41	12.34	14.29	15.21	16.85	17.88	
CO	−26.42	47.21	6.95	7.14	7.61	7.95	8.41	8.67	
CO_2	−94.05	51.08	8.91	10.65	12.32	12.99	13.93	14.44	
HCO	10.40	53.66	8.24	9.28	10.74	11.52	12.56	13.14	
CH_2O	−27.70	52.24	8.40	10.50	13.36	14.88	16.97	18.12	
CH_3	34.82	46.37	9.23	10.83	12.87	14.12	16.27	17.55	
CH_4	−17.90	44.46	8.43	11.14	15.00	17.25	20.63	22.58	
HCOOH	−92.61	59.27	10.71	14.54	18.35	20.07	22.66	23.80	[a]
CH_2OH	−2.13	58.88	11.27	14.59	18.03	19.58	21.92	23.26	[b]
CH_3O	3.90	54.60	9.08	12.43	16.63	18.60	21.51	23.26	
CH_3OH	−48.06	57.27	10.51	14.25	19.07	21.40	25.02	27.25	
HOC_2H_4OH	−92.97	72.90	18.59	26.22	34.21	37.93	44.05	47.67	[c]
C_2H_6	−20.04	54.72	12.58	18.62	25.82	29.30	34.61	37.92	
N_2	0.00	45.77	6.95	7.08	7.50	7.83	8.32	8.60	
Ar	0.00	36.98	4.97	4.97	4.97	4.97	4.97	4.97	

Units: $\Delta H_{f,298}$ (kcal/mol), S_{298}, and c_p (cal/mol K). All values from ref. [40], except as noted.

[a] From ref. [109].

[b] $\Delta H_{f,298}$ from ref. [38].

[c] Specific heat calculated by group additivity, using $\Delta H_{f,298}$ and S_{298} from ref. [109].

pressure. Both cases were calculated in this work and representative points are indicated on the figures as the average parameter with error bars indicating the limiting cases.

The SENKIN program [40] was used to calculate all the preceding three cases, i.e., cases involving static-reactor, flow-reactor, and shock-tube comparisons.

Premixed Laminar Flame Speeds: The Chemkin program PREMIX was used to simulate a freely-propagating, one-dimensional, constant-pressure adiabatic flame. The multicomponent diffusion model was used, and thermal diffusion of H and H_2 was included in the calculations. The windward differencing numerical scheme was used for most of the calculations, due to its superior convergence properties. At the high grid resolution used (approximately 150 nodes within the flame, and 50 in the preheat and post-flame regions), less than 0.5 cm/s difference in calculated flame speed results when using the more accurate but less stable central differencing scheme.

Burner-Stabilized Premixed Flat Flames: Species profiles through several low-pressure, burner-stabilized flames were calculated using PREMIX. The measured temperature profiles were used as inputs to the model due to the unquantified heat losses to the burner. The same diffusion model and numerical parameters were used as for the freely-propagating flame calculations.

RESULTS AND DISCUSSION

Static Reactors

Static reactors are typically used to study low temperature oxidation chemistry, where the reaction time scales are measured in minutes. The principal advantages of these experiments are their simplicity, and essentially unlimited time available for observation of slow reactions. However, the influence of surfaces has long remained difficult to handle for numerical modelers. The experiments are often difficult to control without treatment of surfaces by rigorous cleaning procedures, coating with various substances, and/or "aging" or "seasoning" of the vessels by numerous repetitions (often hundreds) of experiments.

The surfaces interact with the experiments both thermally and chemically. Thermal interaction in-

volves transfer of the reaction enthalpy through the walls of the vessel. For the present work, this effect was treated by assuming a lumped heat capacity model, with an overall characteristic thermal transfer rate. The numerical values used in the calculations were initially estimated based on the thermal diffusivity of the major species and the reported dimensions of the reaction vessels. The details of the chemical/surface interactions are discussed below.

The five static reactor experiments selected for simulation are summarized in Table III. The temperatures studied range from 633 to 873 K, and the initial pressures are atmospheric or below. The reactor surfaces in the experiments were uncoated Pyrex or silica. Fort and Hinshelwood [41] followed the extent of reaction by monitoring the pressure rise due to the decreasing average molecular weight of the reacting mixture. The characteristic thermal time of their reactor vessel was much shorter than the reaction time scale, and nearly isothermal conditions were maintained. This was also the case in the experiments of Bone and Gardner [42], and Bell and Tipper [43]. The primary diagnostic in Bone and Gardner's experiment was also pressure rise, although limited species analysis was performed. Carbon monoxide was the primary product detected, with smaller amounts of formaldehyde, formic acid, carbon dioxide, and an unidentified peroxide. The more detailed species measurements of Bell and Tipper [43] were in agreement with Bone and Gardner's results, although in addition, hydrogen and water were also measured, and the peroxide identified as hydrogen peroxide. A reaction scheme for low-temperature methanol oxidation, involving HO_2 as the primary chain carrier, was also proposed. Cathonnet et al. [44] studied methanol oxidation at higher temperatures as a function of equivalence ratio. Temporal species profiles were measured by gas chromatography, and a detailed reaction mechanism was proposed, which reproduced their measurements with a reasonable degree of accuracy. Finally, in the continuously-stirred static reactor study of Aniolek and Wilk [45], overall reaction rate as a function of temperature, pressure, and equivalence ratio was measured by pressure rise. A single set of species measurements was also reported. Ignition events were observed at fuel-rich conditions.

Initial modeling attempts using the baseline mechanism resulted in poor agreement with all the experimental data, with the calculated reaction time scales being much shorter than measured. Because the mechanism successfully simulated high-pressure flow-reactor experiments at temperatures nearing those in the static reactor studies [21], three possibilities were considered. First, the low-pressure conditions of the static-reactor experiments may open new reaction pathways not considered in the mechanism, or a pressure-dependent rate coefficient may not be adequately specified. However, the lower pressures of the static reactor experiments do not favor gas-phase chain termination reactions, as required to cause an overall decrease in reaction rate. Also, detailed falloff expressions have been incorporated for all relevant reactions. Second, the overall reaction rate measured in the flow reactor experiments may be systematically too high. However, flow reactor experiments are generally less affected by surface reactions than are static reactor experiments, particularly if fluid element residence times in the flow reactor are much shorter than diffusion times to/from the reactor walls. Thus, heterogeneous reactions may play an important role in modifying the chemical rate observed in static reactors from that characteristic of homogeneous gas-phase conditions.

The two main reactions generally assumed to be responsible for the chemical effect of surfaces are loss of hydrogen peroxide and hydroperoxyl radical through heterogeneous termination [43,46]. These reactions were modeled by the overall process:

$$HO_2\ (+\text{wall}) \longrightarrow \tfrac{1}{2}\,H_2 + O_2$$
$$H_2O_2\ (+\text{wall}) \longrightarrow H_2O + \tfrac{1}{2}\,O_2$$

Initial rate constants were estimated by calculating a characteristic diffusion rate, assuming bi-component

Table III Static Reactor Experiments

Experiment	Temp. (K)	Initial Pressure (atm)	Vessel Material	Surface Area/Volume (cm^{-1})
Fort and Hinshelwood [41]	680–736	0.26–0.53	silica	0.9–packed vessel
Bone and Gardner [42]	633–663	1	silica	0.8
Bell and Tipper [43]	703–743	0.26	Pyrex	1.0
Cathonnet et al. [44]	773–873	0.26–0.38	silica	1.3 (not reported, est.)
Aniolek and Wilk [45]	650–700	0.46–0.92	Pyrex	0.65 (stirred reactor)

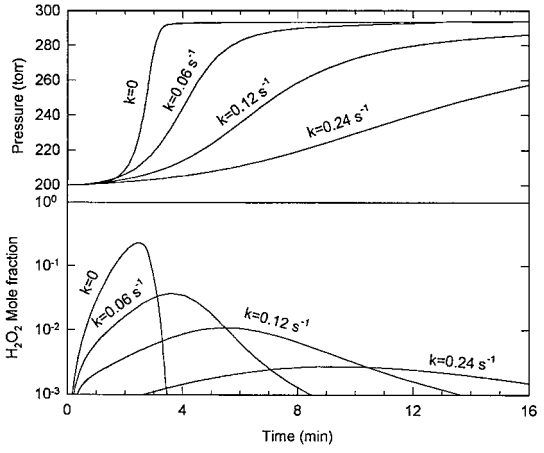

Figure 1 Variation of calculated fuel and hydrogen peroxide profiles for various rate constants of H_2O_2 wall termination. Symbols are measurements, lines are calculated profiles. Data of Bell and Tipper [43]; CH_3OH/O_2, $X_{CH3OH,i} = 0.5$, $T = 713$ K, $p_i = 200$ torr, and $\phi = 1.5$.

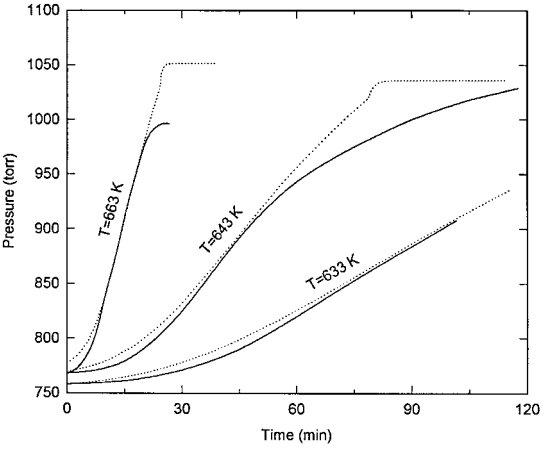

Figure 3 Calculated and measured pressure profiles for static reactor experiments of Bone and Gardner [42]; CH_3OH/O_2, $X_{CH3OH,i} = 0.67$, $p_i = 760$ torr, and $\phi = 3.0$. Hydrogen peroxide wall termination rate constant = 0.028, 0.040, and 0.090 s^{-1} for 633, 643, and 663 K cases, respectively.

diffusion with the major species, and then varied to optimize the comparison to each experiment. The calculated overall reaction rate was found to be extremely sensitive to the rate constant for hydrogen peroxide termination, and quite insensitive to that for hydroperoxyl radical destruction (Fig. 1). Thus, only the H_2O_2 wall reaction effect was included for the final comparisons shown in Figures 2 through 5.

Excellent agreement could be obtained for both species and pressure profiles by this method, with the exception of the experiments of Aniolek and Wilk [45]. Simulation of this experiment was complicated by its nonisothermal nature. Adjustment of the lumped heat transfer rate permitted qualitative reproduction of the observed ignition events, although the exact character of the events was influenced by both the heat transfer and hydrogen peroxide rates. Quantitative calculation of the species profiles was not achieved however. The reported methanol and formaldehyde species profiles exhibited unusual behavior, with apparent

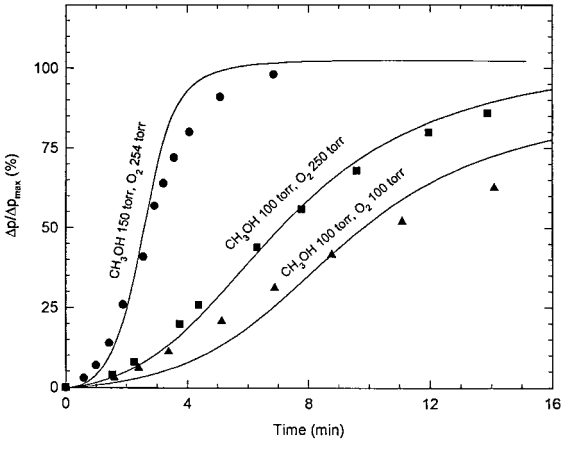

Figure 2 Calculated and measured pressure profiles for static reactor experiments of Fort and Hinshelwood [41]; CH_3OH/O_2 and $T = 710$ K. Hydrogen peroxide wall termination rate constant = 0.080, 0.145, and 0.133 s^{-1} for 400, 350, and 200 torr cases, respectively.

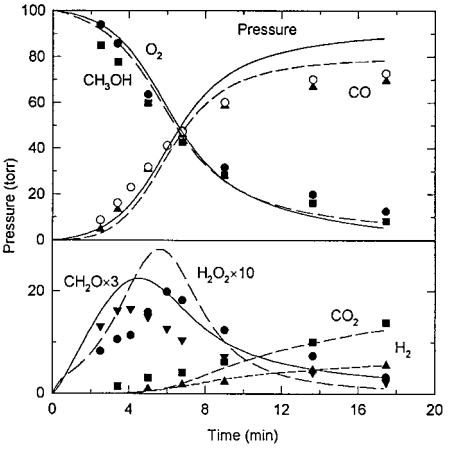

Figure 4 Calculated and measured pressure and species profiles for static reactor experiments of Bell and Tipper [43]. Conditions same as Figure 1. Hydrogen peroxide wall termination rate constant = 0.12 s^{-1}.

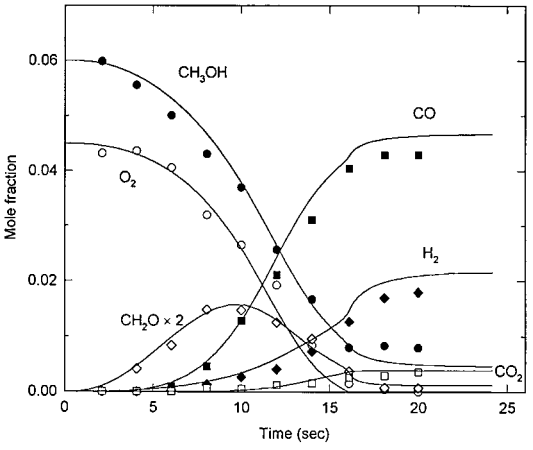

Figure 5 Calculated and measured pressure and species profiles for static reactor experiments of Cathonnet et al. [44]; $CH_3OH/N_2/O_2$, $X_{CH_3OH,i} = 0.06$, $T = 823$ K, $p_i = 200$ torr, and $\phi = 2.0$. Hydrogen peroxide wall termination rate constant $= 0.35\ s^{-1}$.

steady-state values reached early in the reaction. Because the CO and CO_2 mole fractions continued to rise after the methanol and formaldehyde mole fractions had reached approximately steady values, it is likely that a significant amount of those species were adsorbed onto the reactor walls, which were washed with boric acid prior to use. Methanol adsorption onto boric acid-coated walls has been recognized as a significant problem in earlier experiments [46].

The overall low-temperature reaction mechanism is quite simple:

$$CH_3OH + O_2 = CH_2OH + HO_2 \quad \text{(initiation)}$$
$$CH_2OH + O_2 = CH_2O + HO_2 \quad \text{(propagation)}$$
$$CH_3OH + HO_2 = CH_2OH + H_2O_2 \quad \text{(propagation)}$$
$$CH_2O + HO_2 = HCO + H_2O_2 \quad \text{(propagation)}$$
$$HCO + O_2 = CO + HO_2 \quad \text{(propagation)}$$
$$H_2O_2\ (+\text{wall}) \longrightarrow H_2O + \tfrac{1}{2}\,O_2 \quad \text{(termination)}$$
$$H_2O_2 = 2\ OH \quad \text{(branching)}$$
$$CH_3OH + OH = CH_2OH + H_2O \quad \text{(propagation)}$$
$$CH_2O + OH = HCO + H_2O \quad \text{(propagation)}$$

The primary destruction path for methanol is the reaction with HO_2, accounting for 80–90% of the total methanol consumption. The hydrogen peroxide, once formed by the aforementioned reaction, primarily undergoes wall termination. Gas-phase thermal decomposition of hydrogen peroxide was neglected in the conceptual mechanism of Bell and Tipper [43] because its rate constant has been considered to be too slow below 700 K to contribute significantly to the overall reaction. However, although the rate constant drops rapidly with temperature due to its 45 kcal/mole activation energy, the ratio of experimental observation time to H_2O_2 decomposition time remains roughly constant over the set of experiments modeled. Thus the competition between opposing reaction paths remains rate-controlling even below 700 K.

The rate constant for H_2O_2 wall-termination used

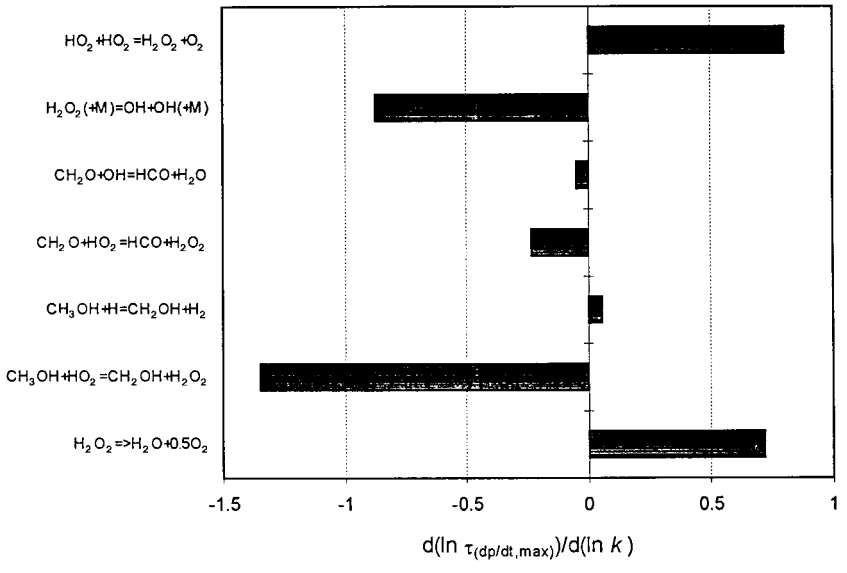

Figure 6 Normalized gradient sensitivity coefficients for time to maximum rate of pressure rise vs. rate constant. Conditions same as Figure 1.

Table IV Flow Reactor Experiments

Experiment	Pressure (atm)	Temperature (K)	$X_{F,0}$	Equivalence Ratio	Residence Time (s)
Aronowitz, et al. [48]					
	1.0	1010	0.00690	0.051	0.120
	1.0	1000	0.00735	1.60	0.080
Norton and Dryer [3]					
	1.0	1027	0.00779	0.59	0.085
	1.0	1030	0.00943	1.22	0.100
	1.0	1034	0.0101	1.58	0.105
Held [21,22]					
	1.0	1043	0.00344	0.86	0.120
	2.5	949	0.00333	0.83	0.33
	2.5	907	0.00333	0.33	0.35
	2.5	911	0.00333	2.17	0.35
	5.0	860	0.00372	0.93	0.75
	5.0	858	0.00372	0.37	0.73
	5.0	857	0.00372	2.32	0.75
	10.0	809	0.00415	1.04	1.6
	10.0	810	0.00415	0.42	1.5
	10.0	811	0.00415	2.60	1.6
	15.0	783	0.00415	1.04	2.4
	15.0	781	0.00415	2.59	2.4
	20.0	752	0.00364	0.93	3.8

in each calculation is listed in the figure captions. The values follow the general trend for a diffusion-controlled process, increasing with temperature, and decreasing with pressure. The rate constants that provided the best fit to the data were lower than the value calculated using the characteristic diffusion rate by about two orders of magnitude, implying a destruction efficiency of about 0.5–1% for H_2O_2 at 700 K for quartz and Pyrex. A comparable destruction efficiency (0.15–0.6%) can be derived from a study of the heterogeneous decomposition of hydrogen peroxide in a quartz tube [47].

Detailed gradient sensitivity analysis results for the conditions of Bell and Tipper are shown in Figure 6. The most sensitive rate constants clearly involve the production and destruction paths for hydrogen peroxide. The peak H_2O_2 mole fraction is also a strong function of its heterogeneous consumption rate. In the absence of such a path, hydrogen peroxide yield exceeds the measured value by over an order of magnitude.

Flow Reactors

Flow reactor experiments essentially bridge the gap between static-reactor and shock-tube experiments for the study of chemical kinetics in the temperature range of 800–1200 K. Most of the methanol oxidation data available previously were obtained at atmospheric pressure, and temperatures ranging from 950–1100 K. Recently, high pressure (up to 20 atm) oxidation data have been reported at temperatures from 750–1100 K, over a range of equivalence ratios. The experimental conditions are summarized in Table IV.

Aronowitz et al. [48] reported species profile data for two experiments, one very fuel-lean (Fig. 7) and one fuel-rich (Fig. 8). The initial temperature was 999 ± 1 K and the pressure was one atmosphere for both experiments. The formaldehyde measurements

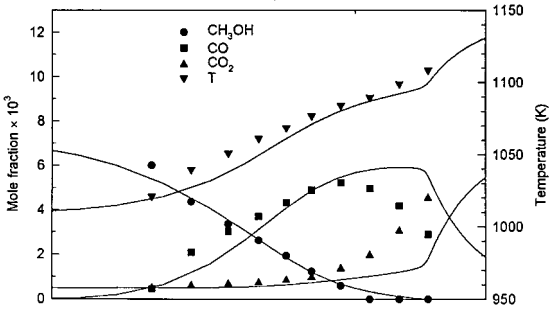

Figure 7 Species and temperature profiles for flow reactor experiments of Aronowitz et al. [48]; $CH_3OH/N_2/O_2$, $X_{CH_3OH,i} = 0.00690$, $T_i = 1010$ K, $p = 1$ atm, and $\phi = 0.051$.

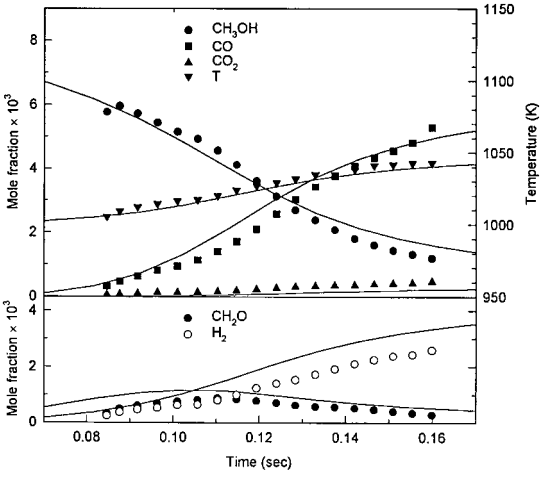

Figure 8 Species and temperature profiles for flow reactor experiments of Aronowitz et al. [48]; $CH_3OH/N_2/O_2$, $X_{CH_3OH,i} = 0.00735$, $T_i = 1000$ K, p = 1 atm, and $\phi = 1.60$.

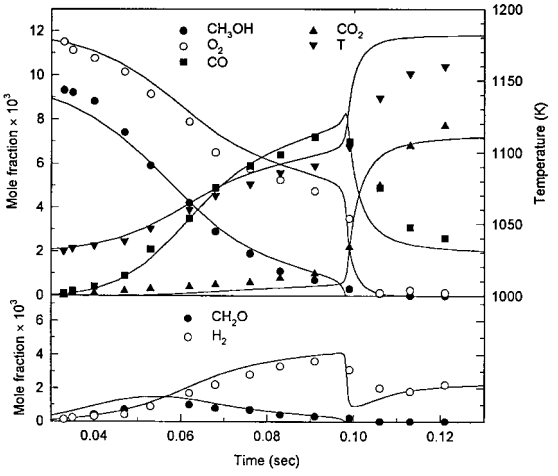

Figure 10 Species and temperature profiles for flow reactor experiments of Norton and Dryer [3]; $CH_3OH/N_2/O_2$, $X_{CH_3OH,i} = 0.00943$, $T_i = 1030$ K, $p = 1$ atm, and $\phi = 1.22$.

were acknowledged to be suspect due to difficulties in obtaining stable samples for off-line gas chromatographic analyses. Norton and Dryer [3] reported three experiments at slightly higher initial temperature (1030 ± 4 K), atmospheric pressure, and covering fuel-lean through fuel-rich equivalence ratios (Figs. 9–11). They reported a "plateau" in the measured temperature profile of the stoichiometric and fuel-rich experiments that was not observed in Aronowitz's experiments. It should be noted, however, that Aronowitz's experiments did not cover a sufficient extent of reaction to observe such a plateau. The detailed model validated against these experiments, as mentioned earlier, forms a basis for the present work. Finally, Held and Dryer's [21] experiments (Figures 12–16) covered a similar equivalence ratio range to Norton and Dryer's [3], but the majority of the data were collected at higher pressures and lower temperatures. The overall behavior of the system was observed to be qualitatively similar to the atmospheric pressure experiments, although the oxidation of CO to CO_2 subsequent to full methanol consumption was observed to

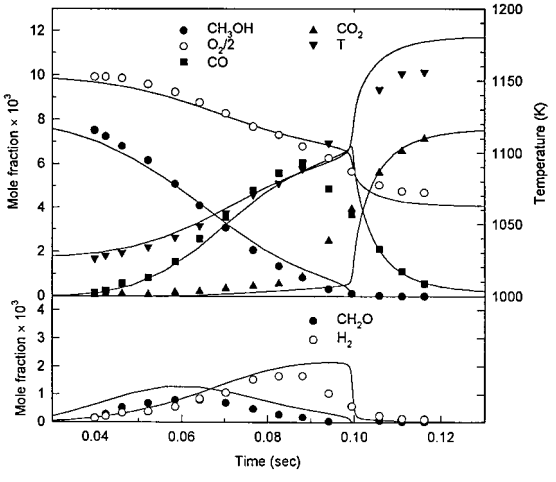

Figure 9 Species and temperature profiles for flow reactor experiments of Norton and Dryer [3]; $CH_3OH/N_2/O_2$, $X_{CH_3OH,i} = 0.00779$, $T_i = 1027$ K, $p = 1$ atm, and $\phi = 0.59$.

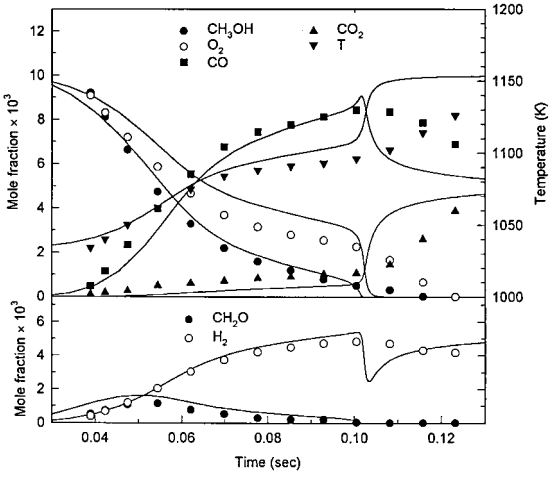

Figure 11 Species and temperature profiles for flow reactor experiments of Norton and Dryer [3]; $CH_3OH/N_2/O_2$, $X_{CH_3OH,i} = 0.0101$, $T_i = 1034$ K, $p = 1$ atm, and $\phi = 1.58$.

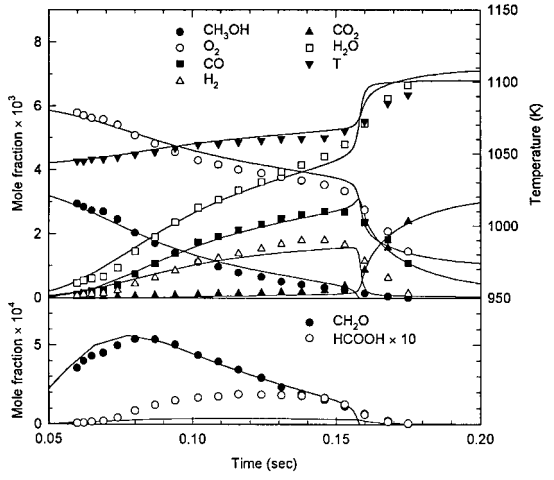

Figure 12 Species and temperature profiles for flow reactor experiments of Held and Dryer [21]; $CH_3OH/N_2/O_2$, $X_{CH_3OH,i} = 0.00344$, $T_i = 1043$ K, $p = 1$ atm, and $\phi = 0.86$.

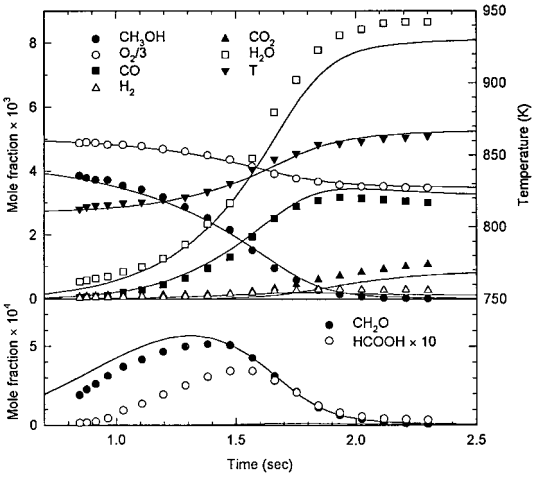

Figure 14 Species and temperature profiles for flow reactor experiments of Held and Dryer [21]; $CH_3OH/N_2/O_2$, $X_{CH_3OH,i} = 0.00415$, $T_i = 810$ K, $p = 10$ atm, and $\phi = 0.42$.

be much slower relative to the oxidation rate of the fuel. Held and Dryer made formaldehyde measurements using continuous sampling and on-line Fourier Transform Infrared (FTIR) monitoring, removing off-line analytical uncertainties present in the works of Aronowitz et al. and Norton and Dryer.

The agreement between the calculated species and temperature profiles (Figs. 12–16) is generally within experimental error. As the temperature increases beyond those of the static reactor experiments, the dominant methanol consumption path becomes

$$CH_3OH + X = CH_2OH + X, (X = OH, H)$$

The hydroperoxyl radical remains a critical influence upon the overall reaction rate, even though it does not contribute significantly to the overall destruction of methanol. Hydrogen peroxide thermal decomposition is an important source of chain-branching, as it was in the static reactor experiments. However, at the higher temperatures and pressures of the flow reactor experiments, the rate of thermal decomposition is much greater than any reasonable wall termination reaction.

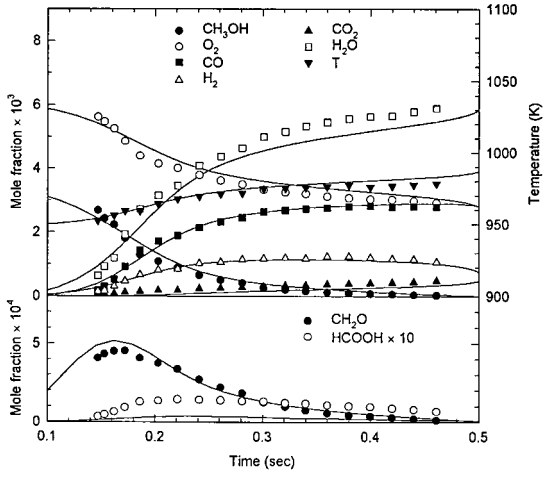

Figure 13 Species and temperature profiles for flow reactor experiments of Held and Dryer [21]; $CH_3OH/N_2/O_2$, $X_{CH_3OH,i} = 0.00333$, $T_i = 949$ K, $p = 2.5$ atm, and $\phi = 0.83$.

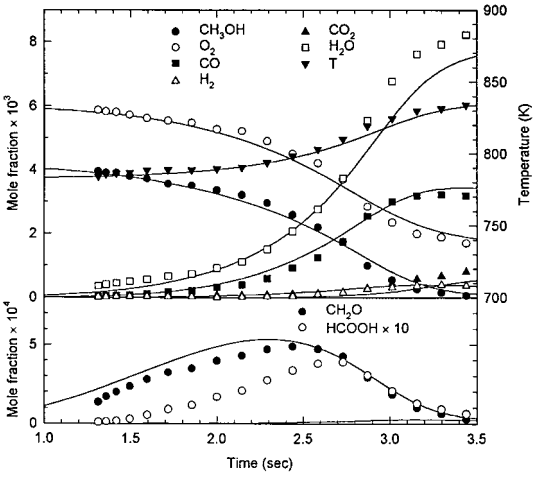

Figure 15 Species and temperature profiles for flow reactor experiments of Held and Dryer [21]; $CH_3OH/N_2/O_2$, $X_{CH_3OH,i} = 0.00415$, $T_i = 783$ K, $p = 15$ atm, and $\phi = 1.04$.

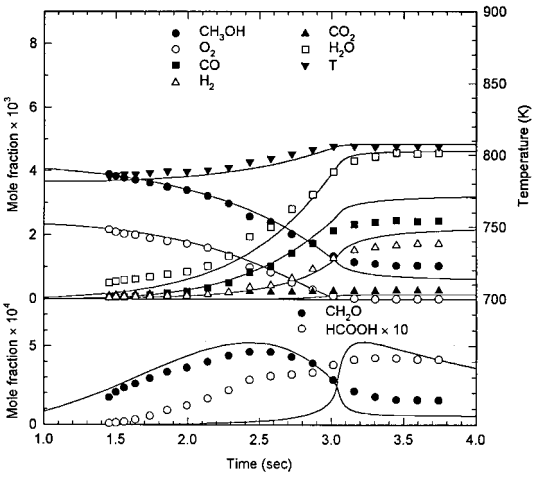

Figure 16 Species and temperature profiles for flow reactor experiments of Held and Dryer [21]; $CH_3OH/N_2/O_2$, $X_{CH_3OH,i} = 0.00415$, $T_i = 781$ K, $p = 15$ atm, and $\phi = 2.59$.

Thus, its rate of formation becomes rate-controlling, rather than its relative decomposition routes. Reactions 25 and 70 provide abundant sources of HO_2 up to at least 1200 K, as the thermal decomposition rates of CH_2OH and HCO are relatively slow below that temperature. Sensitivity analysis results (Fig. 17) show that the rate constant for the pseudo-chain-branching reaction, $CH_3OH + HO_2 = CH_2OH + H_2O_2$ (87), is rate-controlling throughout the range of conditions studied. The competing reaction, $HO_2 + HO_2 = H_2O_2 + O_2$ (14), is effectively straight-chain once H_2O_2 thermal decomposition (15) is considered.

Shock Tubes

Several shock-tube studies of methanol oxidation and pyrolysis extend to temperatures approaching 2200 K. The study by Cooke et al. [49] used OH and CO_2 emission to detect "ignition delay" times for methanol oxidation from 1570–1870 K and 200–300 torr. The effective activation energy for CO_2 emission was 150 kJ/mol, while for OH it was 348 kJ/mol.

Bowman [6] investigated the oxidation of methanol behind reflected shock waves using the maximum emission of 370 nm radiation, attributed to the chemiluminescent reaction of CO and O-atom, to define a characteristic reaction time. The conditions covered an equivalence ratio range of 0.75 to 6.0, a temperature range of 1545 to 2180 K and a density range of 0.92×10^{-5} to 3.02×10^{-5} mol/cm^3. With the excep-

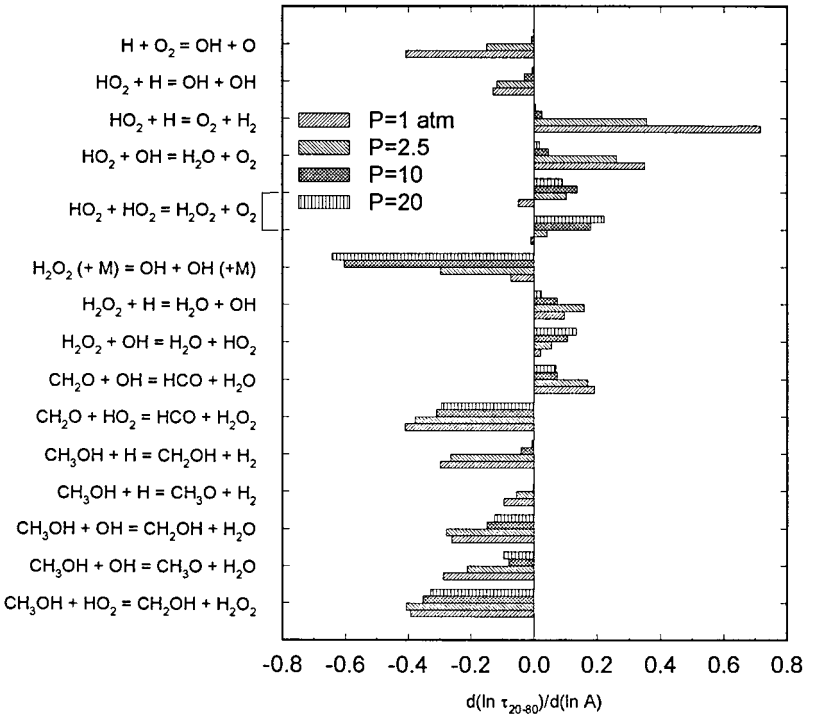

Figure 17 Gradient sensitivity coefficients for time to 50% methanol consumption vs. rate coefficient for the conditions of Held and Dryer.

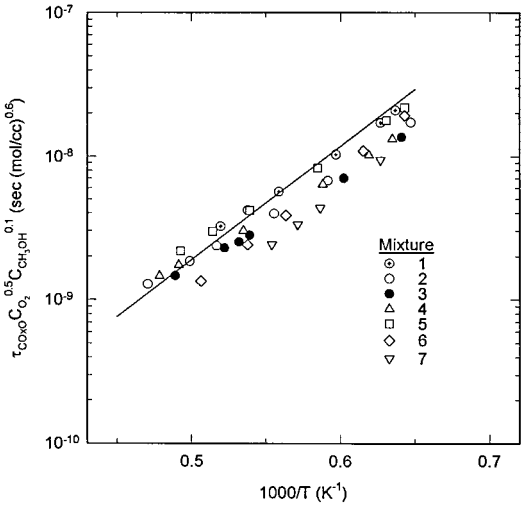

Figure 18 Shock-tube ignition delay calculations for conditions of Bowman [6]. Symbols are calculated ignition delay, as measured by the maximum in $\chi_{CO}\chi_{O}$. Line is correlation based on experimental results.

tion of the most fuel rich case, the experimental data were well correlated by the expression

$$\tau_{CO\times O} C_{O_2}{}^{0.5} C_{CH_3OH}{}^{0.1} = 2.1 \times 10^{-13} \exp(151.5\text{kJ}/RT)\text{sec} \cdot (\text{mole/cm}^3)^{0.6}$$

A detailed kinetic mechanism, initially comprising 28 reactions among 14 species and later reduced to 19 reactions, was proposed. Although the agreement between the model and experiment was reasonable at the highest temperatures, it degraded rapidly below 1800 K.

Tsuboi and Hashimoto [50] studied the oxidation of methanol from 1200–1800 K at relatively high dilution, $(X_{CH_3OH})_0 \leq 0.02$. A detailed mechanism was proposed to correlate the fuel, oxygen, density, and temperature dependencies.

Cribb et al. [51] used laser schlieren and mass spectrometric techniques to characterize the high-temperature oxidation of methanol. A detailed model was proposed that performed well against the laser schlieren profiles was excellent, but was in significant discrepancy with the species data.

Due to the wide ranges in temperature and equivalence ratio of the Bowman experiments, these data were selected as the primary test case for the present mechanism. The maximum 370-nm light emission ($\equiv \tau_{CO\times O}$) was assumed to occur at the maximum in the product of the CO and O-atom mole fractions. The computational results, which appear as the symbols in Figure 18, were converted to the form used in Bowman's correlation. The solid line is the experimental temperature dependence of the correlation expression. The agreement is slightly outside the experimental uncertainty, particularly at the lower temperatures of the study (1550–1700 K). A number of possible reasons for this discrepancy were explored, including the physical model (constant pressure vs. constant volume), the uncertainty in initial temperature, and the reaction mechanism. The difference in calculated $\tau_{CO\times O}$ between constant pressure and volume models is less than 10%. While applying the ± 50 K initial temperature uncertainty to the model initial conditions does make the model predictions closer to the experimental values, the temperature error would have to be systematically low.

Detailed sensitivity analysis was applied to determine the most likely reaction rate coefficients which might contribute to the discrepancy. The linear sensitivity coefficients pointed to unreasonably large changes in rate coefficients in most cases if a single rate constant was to be varied. Second-order sensitivity analysis likewise did not reveal significant two-factor interactions that could bring the model into closer agreement with the experiment. The second-order analysis did, however, indicate that the sensitivity coefficient for reaction (10),

$$HO_2 + H = H_2 + O_2 \qquad (10)$$

was highly nonlinear. By trial and error, it was found that an increase in the rate coefficient of approximately a factor of three would bring the low-temperature shock-tube calculations into excellent agreement with the experiments. The reaction of hydroperoxyl with H-atoms has been studied only at relatively low temperatures (<800 K), and was found to be dominated by the product channel OH + OH. Recently, the rate constant for the analogous reaction

$$HO_2 + OH = H_2O + O_2 \qquad (13)$$

was determined to exhibit highly non-Arrhenius behavior at similar temperatures to those of interest here [52], due to a transition from a chemically activated complex reaction at lower temperatures to a higher-activation energy direct abstraction route above 1000 K. Much improved results can be obtained by assuming a similar channel for reaction (10) (Fig. 19), using the same rate constant as measured for reaction (13). Due to the highly speculative nature of such an assumption, this rate modification was not incorporated into the mechanism reported in Table I.

At high temperatures, methanol is consumed primarily through abstraction by both H and OH. At the

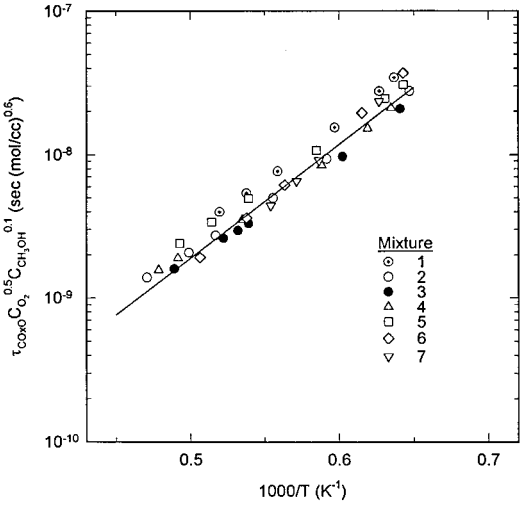

Figure 19 Same calculations as Figure 18, with high-temperature rate constant for $HO_2 + H = H_2 + O_2$.

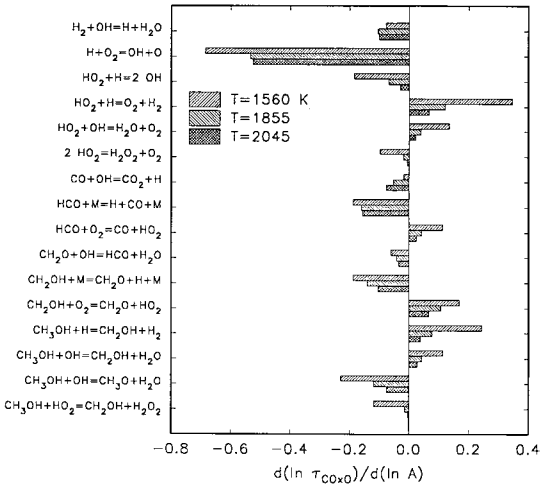

Figure 20 Gradient sensitivity coefficients of ignition delay time to rate coefficient for the conditions of Bowman's Mixture 3.

most fuel-lean conditions, O-atom abstraction becomes more important, while the abstraction rate by H-atoms decreases. Under most conditions, however, the overall rate of fuel consumption is not controlled by the rate coefficients of either these reactions or the initiation reaction. The relative stability of the hydroxymethyl radical results in an appreciable rate for its reaction with molecular oxygen, even at temperatures in excess of 1500 K. The hydroperoxyl radical plays an important role in methanol oxidation well into the high temperature kinetic regime, often demarcated by conditions where the ratio of $k_1/k_9[M]$ is greater than order 1.

The results of the gradient sensitivity analysis are consistent with the suspected importance of HO_2 in the mechanism (Fig. 20). For the conditions of Mixture 3, the six most sensitive reactions are, in order of their peak sensitivity coefficients for $\tau_{CO\times O}$,

$$(-) \qquad H + O_2 = OH + O \qquad (1)$$

$$(-) \qquad HCO + M = H + CO + M \qquad (24)$$

$$(-) \qquad CH_2OH + M = CH_2O + H + M \qquad (65)$$

$$(+) \qquad HO_2 + H = O_2 + H_2 \qquad (10)$$

$$(-) \qquad CH_3OH + OH = CH_3O + H_2O \qquad (84)$$

$$(+) \qquad CH_2OH + O_2 = CH_2O + HO_2 \qquad (70)$$

The $+/-$ signs indicate whether an increase in the reaction rate increases or decreases $\tau_{CO\times O}$. The most sensitive reaction is the well known branching reaction (1). The relative sensitivity of the other reactions may be understood on the basis of their effect on the supply of H-atoms to the branching reaction.

The formyl radical decomposition reaction is the main supply route of H-atoms. This fact alone does not make it a sensitive reaction. The important point is that other, less reactive product paths are available for HCO, such as $HCO + O_2$ (25) and HCO + H (26). The availability of these alternative reaction paths makes the rate of formyl radical decomposition very important.

Despite the high temperatures of the shock-tube experiments, HO_2 is still an important species. Its role is considerably different than at lower temperatures exceeding about 800 K, where it acts primarily as a chain carrying species, through hydrogen peroxide formation and decomposition. At high temperature, its primary effect is to provide a termination pathway for H-atoms, through reaction (10).

The pair of hydroxymethyl (65,70) reactions are in direct competition with each other. The decomposition reaction (65) produces H-atoms that go on to reaction (1). The reaction with molecular oxygen (70), although relatively slow at these high temperatures, is strongly inhibiting for two reasons. First, it indirectly depletes the system of H-atoms otherwise produced through reaction (1). Second, it produces HO_2 that contributes to the termination reaction (10).

It is interesting to compare the shock-tube conditions to those of the atmospheric-pressure flow-reactor experiments. Although the temperature and pressure of the flow-reactor experiments place them above the extended second explosion limit for hydrogen, reaction (1) is relatively unimportant as long as methanol and formaldehyde remain. Below 1500 K, these abstraction reactions are considerably faster than the branching reaction. The activation energies of these reactions are approximately 2–6 kcal/mol for abstraction, compared to 17 kcal/mol for reaction (1). Above

1500 K, reaction (1) is now fast enough relative to these abstraction reactions to exert a large influence on the reacting system. At 2000 K and above, the branching reaction is by far the dominant influence.

Premixed Laminar Flames

A large number of studies have focused upon premixed methanol-air and methanol-oxygen-argon laminar flames, both experimentally and computationally. The experimental work can be essentially divided into two categories. The first is the determination of laminar flame speed as a function of equivalence ratio, initial temperature and/or pressure, using various techniques: propagation rate in a horizontal tube [53], a Bunsen flame area method [54], spherical constant-volume bomb [55,56], and twin opposed jet counterflow flame [5]. The second category involves the use of low-pressure flat-flame burner experiments to observe the temperature and species profiles within the flame structure. Temperatures are typically determined using radiation-corrected thermocouple measurements. Species profiles are typically determined by quartz microprobe sampling and gas chromatography for stable species [9,10,57], molecular beam sampling mass spectrometry for both stable and radical species [7,8,58,59], and/or electron spin resonance for H, O and OH [9,60].

A number of detailed kinetic schemes have been proposed to account for both the parametric variations in laminar burning velocity [5,12,13,61,62] and the measured species profiles for the burner stabilized flames [10,58,59,63]. The mechanisms are, in most cases, modifications of either the Westbrook and Dryer [1] or Dove and Warnatz [62] mechanisms.

The purpose of the present modeling comparisons with experiments is not to refine the present mechanism or its rate expressions, but to compare calculated results apriori with data on flame speed data and flame temperature/species profiles. The additional complexity arising from the varying temperature-time history and the presence of strong diffusive fluxes in flames compromises the isolation of individual chemical reaction effects. Rather, it is the intent of this section to demonstrate reasonable agreement between measured flame speeds and a mechanism based on fundamental kinetic experiments, and then, through study of the model, to identify reactions that influence the calculated flame speeds using sensitivity and reaction path analyses.

Premixed Laminar Flame Profiles

Three sets of low-pressure burner-stabilized flat flame data are available in the literature. Vandooren and Van Tiggelen performed molecular beam mass spectrometric analysis of three methanol flames with oxygen, argon and/or hydrogen at 40 torr [7,8]. The measured species profiles included the major and minor stable species, as well as H, O, OH, and CH_3O (a combination of methoxy and hydroxymethyl radicals). Pauwels, et al. [9] studied a stoichiometric methanol/air flame at 80 torr, with stable species measurements by gas chromatography, and H, O, and OH by electron spin resonance. Bradley et al. measured burning velocities over a range of pressures and equivalence ratios, but only report major species profiles using gas chromatography for a single set of conditions (no radical species were measured). Here, comparisons were made with the data set of Vandooren and Van Tiggelen because of its comprehensive character.

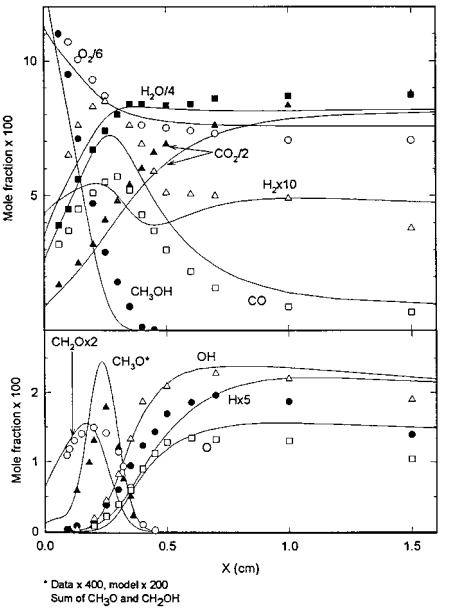

Figure 21 Calculated and measured species profiles for Flame II of Vandooren and Van Tiggelen [8] (v_0 = 44 cm/s, $X_{CH_3OH,i}$ = 0.194, $X_{O_2,i}$ = 0.806, T_0 = 298 K, and p = 0.0526 atm).

The comparison between the experimental data and model calculations for Vandooren and Van Tiggelen's Flame II are shown in Figure 21. The agreement with the other two flames which were studied experimentally is similar. Some relative spatial shift of the profiles is evident near the burner surface. This effect may be due to disturbance of the flame by the MBMS sampling cone. The only species profiles in significant disagreement are hydrogen and "CH_3O" (the summation of the methoxy and hydroxymethyl radical mole fractions). Sensitivity analysis indicates that the H + O_2 branching reaction (1), H_2 + OH abstraction reaction (3), and the branching ratio between the HO_2 + H re-

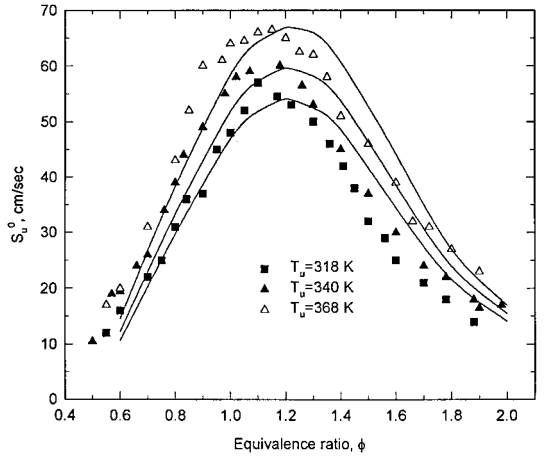

Figure 22 Calculated and measured premixed laminar flame speeds for methanol/air, 1 atm. Data from Egolfopoulos et al. [5].

action product channels (10 and 11) are the predominant influences on the molecular hydrogen mole fraction. Given the relative uncertainty in the rate constants for these reactions, the HO_2 + H branching ratio appears a likely source for the discrepancy. As in the shock-tube modeling, an increased rate constant for the H_2 + O_2 product channel (factor of three) gives significantly improved results.

The "CH_3O" profile is over-predicted by a factor of about 2.5 for all three flames. The methoxy radical is calculated to be the dominant species in the flame due to its relatively slow reaction with oxygen relative to hydroxymethyl. The branching ratio between CH_3OH + OH product channels (83 and 84) is the main influence on the peak "CH_3O" mole fraction, with lesser contributions from the rate constants of CH_3O + O_2 (47) and CH_3O thermal decomposition (42). In view of the experimental difficulty in making an accurate calibration and measurement of CH_3O, the current discrepancy does not warrant alteration of the rate constants of these reactions.

Premixed Laminar Flame Speeds

The calculated results at three different initial mixture temperatures are shown in Figure 22 along with the experimental data of Egolfopoulos et al. [5]. The authors calculated the nominal flame speed by extrapolating the function of measured flame speed versus stretch rate linearly to stretch-free conditions. Recent investigations indicate that the assumption of a linear dependence is slightly in error, making the reported flame speeds in Reference [5] less certain than first believed [64]. However, the experimental technique is superior to alternative ones, and thus the data are used as the standard of comparison here.

The calculated flame speeds are in reasonable agreement with the lean and stoichiometric data at both initial temperatures. The calculated flame speeds for fuel rich conditions are approximately 10% in excess of the measurements, although the disagreement is less severe at the most fuel rich conditions. The maximum calculated flame speed occurs at an equivalence ratio of approximately 1.2, versus the experimental value of 1.1, although the calculated maximum flame speeds agree very well. The estimated uncertainty in the laminar flame speed measurements is about ± 3 cm/sec, of which ± 1 cm/sec is from the LDV technique, and an additional ± 2 cm/s is estimated from a 95% confidence band with the scatter of the data around a smoothed curve. The uncertainty in reported equivalence ratio is more difficult to evaluate, but at the very low liquid-fuel flows required for these experiments, a value of $\pm 3-5\%$ is not at all unlikely. The effect of radiative heat loss from the flame was evaluated using a simple radiation model in PREMIX, using Plank mean absorption coefficients for CO_2 and H_2O. The change in flame speed was in general negligible. Finally, the aforementioned linear stretch assumption could systematically reduce the measured flame speeds by about $1-2$ cm/sec, based on methane flame speed measurements under similar conditions [64]. Considering these uncertainties, the agreement with the lean flame speeds is within the error band of the data. Under fuel-rich conditions, the calculated flame speeds may be beyond the uncertainty limits.

Reaction Path Analysis

The contribution of individual reactions to the chemical production and destruction rates is calculated by integration of the instantaneous production rate of species i due to reaction j across the computational domain:

$$\omega_{ij} = \int_{-\infty}^{+\infty} \dot{\omega}_{ij} \cdot dt = \int_{-\infty}^{+\infty} \frac{\dot{\omega}_{ij}}{v} \cdot dx$$

where:

$\omega_{ij} \equiv$ total net chemical production of species i by reaction j (mol cm^{-3})

$\dot{\omega}_{ij} \equiv$ instantaneous net chemical production rate of species i by reaction j (mol cm^{-3} s^{-1})

$v \equiv$ local fluid velocity

These values describe the reaction path through which the fuel is ultimately converted to products.

The abstraction reactions 80–84 consume the majority of the fuel. The two reactions involving OH (83 and 84) are dominant throughout the range of stoichiometry studied, being responsible for between 46 and 66% of the fuel consumption, depending on the equivalence ratio. As the fuel mixture varies from fuel lean to rich, the abstraction reaction by H-atoms takes on increasing importance, consuming up to 35% of the methanol at an equivalence ratio of 1.4. The reaction with O-atoms accounts for most of the remainder of the fuel consumption pathway, from 8 to 18% of the total as the stoichiometry shifts from rich to lean.

The subsequent fates of the two CH_3O isomers are similar to those described for lower temperature situations, with thermal decomposition of CH_2OH increasing in importance as the temperature rises. Offsetting this trend, to some degree, is the considerably higher oxygen concentration in the flame compared to shock-tube and reactor conditions investigated earlier in this article. Even in a stoichiometric flame, the reaction of hydroxymethyl with oxygen (70) consumes 16 times more CH_2OH than the thermal decomposition reaction (65). Despite the elevated O_2 levels, the methoxy radical still predominantly undergoes decomposition, rather than reaction with oxygen. These two distinct fates contribute to a strong dependence of the calculated flame speed on the branching ratio, $k_{83}/(k_{83} + k_{84})$, seen in Figure 23. Because the methoxy radical primarily produces H-atoms that may become branching agents through reaction (1), while the hydroxymethyl produces HO_2 that predominantly reacts with H-atoms in either a straight chain (11) or terminating (10) reaction, preferential formation of methoxy radical increases the calculated flame speed.

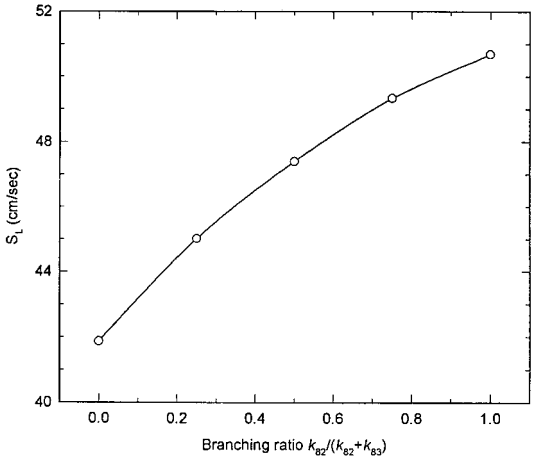

Figure 23 Dependence of methanol/air premixed laminar flame speed on branching ratio for $CH_3OH + OH$ reaction products, $k_{83}/(k_{83} + k_{84})$. 1 atm and 298 K initial conditions.

Sensitivity Analysis

The normalized first-order gradient sensitivity coefficients of the flame speed are depicted in Figure 24 for the most sensitive reactions under lean, stoichiometric, and rich conditions. The initial conditions for these calculations are atmospheric pressure and 298 K. Clearly, the flame speed is dependent on a large number of kinetic parameters in comparison to the reactor, static-reactor, and shock-tube conditions. The $H + O_2$ branching (1) and termination (9) reactions and the CO oxidation reaction (22) are quite important. As in the other high temperature studies, the reason that most of the remaining reactions in Figure 24 have high sensitivity coefficients may be understood from the standpoint of their effect on the supply of H-atoms to reaction (1).

Of the remaining reactions, the formyl radical decomposition reaction (24) displays the strongest positive sensitivity coefficient. Reaction flux analysis shows that formyl decomposition is the largest source of H-atoms to the system, aside from $CO + OH = CO_2 + H$ (22). The decomposition rate is particularly sensitive for flame conditions, because of the high-radical concentrations within flames. The competing reactions, $HCO + H = CO + H_2$ (26) and $HCO + OH = CO + H_2O$ (29), provide alternative, terminating paths for formyl radical consumption. As in the other conditions, abstraction by oxygen (reaction 25) is also a competing process, since it results in a less reactive radical propagating path that becomes relatively more important as the initial oxygen concentration is increased.

An unfortunate circumstance resulting from the high sensitivity of reaction (24) is the effects of uncertainties in the collisional efficiencies for this reaction, particularly for water (present in these flames at mole fractions as high as 0.15 to 0.20). A series of calculations of the flame speed for a 340 K, 1 atmosphere, stoichiometric methanol-air mixture were performed, varying only the enhanced collisional efficiency of water for reaction (24). The results, depicted in Figure 25, clearly demonstrate the strong effect that this parameter exerts on the calculated flame speed. By taking the slope of the logarithmic plot of this function, a sensitivity coefficient of $\partial (\ln S_L)/\partial (\ln \eta_{H_2O}) \approx 0.09$ is obtained. Calculations at other conditions yielded similar coefficients. This magnitude of this normalized sensitivity is approximately half that for the $H + O_2$ branching reaction (1), the most important reaction in determining the flame speed. The collisional efficiency of 3.0 determined from Figure 25 was used throughout this work. It should be noted that the sensitivity of the calculations to this parameter is lim-

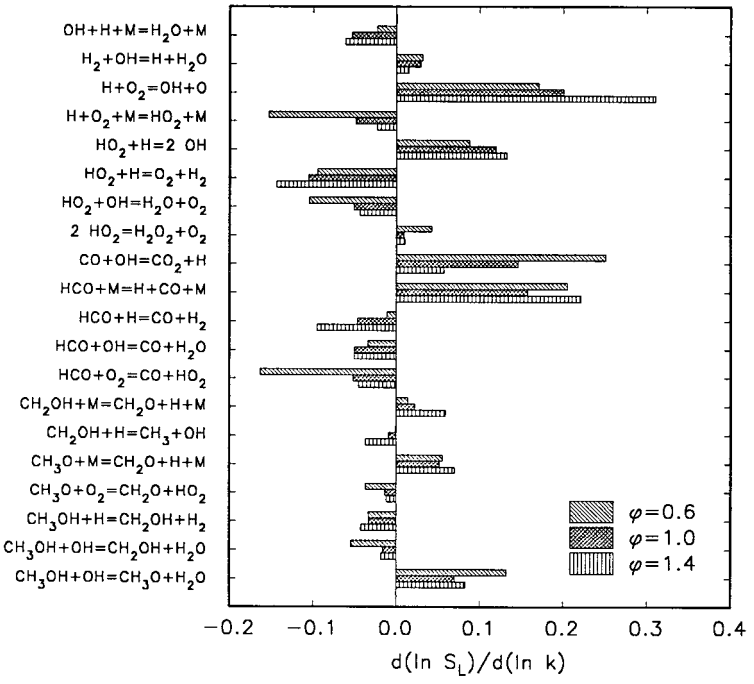

Figure 24 Gradient sensitivity coefficients for methanol/air premixed laminar flame speed vs. rate coefficient. 1 atm, 298 K initial conditions.

ited to the flame studies primarily as a result of the high water content in the reaction zone. The shock-tube and flow-reactor studies were performed for far more dilute conditions, and the static reactor experiments are conducted at low enough temperatures such that formyl radical thermal decomposition is not an important reaction path.

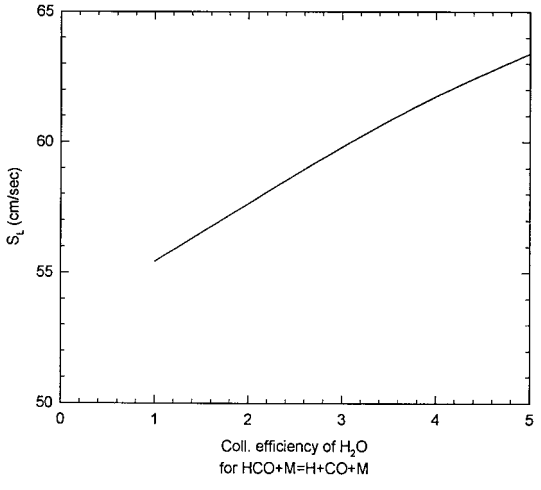

Figure 25 Dependence of methanol/air premixed laminar flame speed on H_2O collisional efficiency for HCO + M = H + CO + M. 1 atm, 340 K initial conditions.

The hydroxymethyl and methoxy radical decomposition reactions (65 and 42) are secondary sources of H-atoms and have less reactive competing destruction paths (67 and 47). The former reaction ($CH_2OH + H = CH_3 + OH$) is of particular interest because of its relatively strong influence at rich equivalence ratios. This reaction has been identified as a significant source of methyl radicals in methanol pyrolysis (2). The only studies of the reaction $CH_2OH + H \rightarrow$ products are those of Hoyermann and co-workers [65,66], who used a discharge fast flow-reactor and mass-spectrometric techniques at low-pressure and ambient temperature. At these conditions, the contribution of the disproportionation reaction (66) was approximately 75%, while the later study confirmed the remainder proceeded through reaction (65). However, these results are unlikely to be directly applicable at combustion temperatures.

The rate constant of reaction (65) has been calculated in other studies by specifying the reverse reaction rate constant and the thermochemistry of the involved species. These values require reevaluation in light of the revised heat of formation of hydroxymethyl [38]. The inclusion of reaction (−65), with a rate constant of approximately 1.8×10^{13} at 2000 K, was necessary to obtain good agreement with H- and O-atom profiles in methane shock-tube experiments [67]. With the revised heat of formation, the K_c for this reaction is

0.0817, giving $k_{65} = 2.2 \times 10^{14}$ at 2000 K. Dombrowsky et al. [23] used a temperature independent rate constant of 1.5×10^{13} for reaction (−65), while Grotheer et al. [13] have adopted a fit that yields a value of 1.9×10^{13} at 2000 K. These values again correspond to very high rate constants for reaction (65), from $1.8-2.3 \times 10^{14}$. In his review, Tsang [26] assumes that the disproportionation process occurs at a rate comparable to that of the ethyl radical and hydrogen. Tsang also assumes the reaction proceeds via addition to form an activated complex $[CH_3OH]^*$, which may undergo either collisional stabilization to form methanol or decomposition to methyl and hydroxyl radicals. The total rate constant is 9.64×10^{13}(cm^3-mol^{-1}-s^{-1}). The decomposition reaction is dominant at most flame conditions, consistent with the reverse rate constant of reaction (79).

At the present time, the recommended rate constants of Tsang [26] are used for reactions (65) and (66) without consideration of the pressure dependence of the rate of reaction (65). Better agreement with the rich flame speed data can be obtained through the use of the higher rate constants for reaction (65); however, these values appear unreasonably high and are not utilized here. None of these expressions reproduces the complex temperature and pressure variation of the activated complex reactions; this is clearly an area requiring further elementary kinetic study.

The two OH abstraction reactions of methanol (83 and 84) display opposing sensitivities, consistent with the aforementioned dependence of the flame speed on the branching ratio. Interestingly, the signs of the sensitivity coefficients for these two reactions are opposite those of the earlier study of Egolfopoulos et al. [5]. In the present mechanism, the reaction producing the methoxy radical (84) displays a positive sensitivity coefficient, indicating that an increased formation rate of this species increases the calculated flame speed. This result is intuitively reasonable, since the primary fate of the methoxy radical yields an H-atom, while the alternative hydroxymethyl radical mainly produces HO_2. The reversed sensitivity coefficients of Egolfopoulos et al. [5] result from their incorrect specification of the reaction products of $CH_3 + OH = CH_2OH + H$ as $CH_3O + H$. The methoxy radical behaves unreasonably as an efficient H-atom sink in their mechanism; thus, increasing its production rate results in a reduced calculated flame speed. Changing the products of this reaction to (the correct products of) $CH_2OH + H$ changes the calculated flame speed using the mechanism of from near 45 cm/sec to greater than 63 cm/s at 298 K, 1 atm.

An additional complicating effect when modeling flames is the importance of molecular diffusion. In particular, H-atom diffusion plays an important role because of its low molecular weight, and, therefore, high diffusion velocity, and its effect on radical branching. Variation of the binary diffusion coefficient of H-atom with nitrogen yields a calculated sensitivity coefficient, $d(\ln S_L)/d(\ln D_{H,N_2})$ that varies from 0.12 at $\phi = 0.8$ to 0.20 at $\phi = 1.4$. These values are comparable to those for sensitive reactions, although the uncertainty in diffusion coefficients is perhaps less than that of a typical reaction rate constant. The sensitivity coefficients for other species diffusion coefficients were also calculated for the 298 K, 1 atmosphere conditions. Other species besides H-atom with sensitivity coefficients greater than 0.05 are H_2O (0.13), OH (0.063), and O_2 (0.054). Thus, species diffusion represents an additional uncertainty in the accurate calculation of flame speeds.

SUMMARY AND CONCLUSIONS

The present model is reasonably successful of reproducing measurements from four different types of experiments, over a wide range of temperature, pressure, and equivalence ratio. The static-reactor experiments were very sensitive to an assumed wall destruction rate constant for H_2O_2, while wall termination for HO_2 at a reasonable rate was found to have an insignificant effect on the overall kinetics. The flow-reactor data were well-predicted without including wall effects. The formic acid formation mechanism was unsuccessful in capturing the dependence of formic acid mole fraction on equivalence ratio. The shock-tube ignition delay calculations fell within experimental error of the correlating parameter developed by Bowman [6], although the calculated delay times at the lower temperatures of the study were systematically too short. The hypothesized increase in the rate constant for $HO_2 + H = H_2 + O_2$ at high temperatures collapses the delay times on the correlation curve, but the absence of measurements of this rate constant at high temperature prohibits its use at present. Finally, the rate constant and reaction channels for the $CH_2OH + H =$ (products) reaction requires additional study. This reaction strongly affects the fuel-rich kinetics of methanol oxidation, and may provide the primary source of C_2 hydrocarbons through the $CH_3 + OH$ channel, followed by CH_3 recombination.

Although the present article has not discussed comparisons of calculations with diffusion flame results, the detailed kinetic model presented here has been utilized extensively at Princeton for the prediction of spherically symmetric, isolated methanol, and methanol/water droplet combustion in both nitrogen/oxygen

and helium oxygen atmospheres [68–72]. These calculations embody full multi-component diffusive transport utilizing the same approach as that employed in the premixed flame calculations reported here. In addition, detailed liquid transport [68], chemiluminescent flame emission [69], and spectral radiative transport effects [71] have been investigated using methanol droplet combustion. Transient droplet burning rate, flame stand-off, and droplet burning extinction phenomena compare favorably with microgravity experiments performed using unsupported droplets [71] in ground-based droptower facilities and with fiber supported droplet experiments performed in a glovebox experiment aboard the Space Shuttle [72]. The reader is referred to these publications for detailed results and discussions regarding calculated flame structure and chemical aspects of droplet diffusion flames employing the present mechanism. Clearly these studies can lead to stringent tests for reduced mechanisms describing chemical kinetics for methanol oxidation under diffusive burning conditions.

Further application of this mechanism within other venues will provide both additional validation of the kinetic scheme, and also understanding of other fundamental processes, such as autoignition in rapid compression machine experiments [73] and spark-ignition engines [14].

The authors would like to acknowledge the assistance of Dr. Richard Yetter for helpful discussions regarding the H_2/O_2 submechanism. This work was supported by a National Science Foundation Fellowship (TJH), and by the U.S. Department of Energy, Chemical Sciences Division, Office of Basic Energy Sciences, under Contract #DE-FG02-86ER-13503.

BIBLIOGRAPHY

1. C. K. Westbrook and F. L. Dryer, *Combust. Sci. and Tech.,* **20,** 125 (1979).
2. T. S. Norton and F. L. Dryer, *Int. J. Chem. Kinet.,* **22,** 219 (1990).
3. T. S. Norton and F. L. Dryer, *Combust. Sci. and Tech.,* **63,** 107 (1989).
4. T. S. Norton, *The Combustion of Simple Alcohol Fuels,* Ph.D. dissertation, Princeton University, 1989.
5. F. N. Egolfopoulos, D. X. Du, and C. K. Law, *Combust. Sci. and Tech.,* **83,** 33 (1992).
6. C. T. Bowman, *Combust. Flame,* **25,** 343 (1975).
7. J. Vandooren, V. P. Balakhin, and P. J. Van Tiggelen, *Arch. Combust.,* **1,** 229 (1981).
8. J. Vandooren and P. J. Van Tiggelen, *18th Symp. (Int.) Combust.,* 473 (1981).
9. J. F. Pauwels, M. Carlier, P. Devolder, and L. R. Sochet, *Combust. Sci. and Tech.,* **64,** 97 (1989).
10. D. Bradley, G. Dixon-Lewis, S. El-Din Habik, L. K. Kwa, and S. El-Sherif, *Combust. Flame,* **85,** 105 (1991).
11. H. H. Grotheer and T. Just, *Combust. Sci. and Tech.,* **91,** 15 (1993).
12. H. H. Grotheer and S. Kelm, Seminar on Flame Structure, 1989.
13. H. H. Grotheer, S. Kelm, H. S. T. Driver, R. J. Hutcheon, R. D. Lockett, and G. N. Robertson, *Ber. Bunsenges. Phys. Chem.,* **96,** 1360 (1992).
14. H. S. T. Driver, R. J. Hutcheon, R. D. Lockett, G. N. Robertson, H. H. Grotheer, and S. Kelm, *Ber. Bunsenges. Phys. Chem.,* **96,** 1376 (1992).
15. F. L. Dryer, in *Fossil fuel combustion: A sourcebook,* W. Bartok and A. F. Sarofim, Eds., Wiley, New York. 1991.
16. R. A. Yetter, F. L. Dryer, and H. Rabitz, *Combust. Sci. and Tech.,* **79,** 97 (1991).
17. T. J. Kim, R. A. Yetter, and F. L. Dryer, (1995). The H_2/O_2 system: High pressure studies and comprehensive reaction mechanism development. *Combust. Sci. and Tech.,* in preparation.
18. T. J. Kim, R. A. Yetter, and F. L. Dryer, *25th Symp. (Int.) Combust.,* 759 (1994).
19. S. Hochgreb, R. A. Yetter, and F. L. Dryer, *23rd Symp. (Int.) Combust.,* 171 (1990).
20. S. Hochgreb and F. L. Dryer, *Combust. Flame,* **91,** 257 (1992).
21. T. J. Held and F. L. Dryer, *25th Symp. (Int.) Combust.,* 901 (1994).
22. T. J. Held, *The oxidation of methanol, isobutene and methyl tertiary-butyl ether,* Ph.D. dissertation, Princeton University, 1993.
23. C. Dombrowski, A. Hoffman, M. Klatt, and H. G. Wagner, *Ber. Bunsenges. Phys. Chem.,* **95,** 1685 (1991).
24. Y. Hidaka, T. Oki, H. Kawano, and T. Higashihara, *J. Phys. Chem.,* **93,** 7134 (1989).
25. K. Spindler and H. G. Wagner, *Ber. Bunsenges. Phys. Chem.,* **86,** 2 (1982).
26. W. Tsang, *J. Phys. Chem. Ref. Data,* **16,** 471 (1987).
27. W. P. Hess and F. P. Tully, *J. Phys. Chem.,* **93,** 1944 (1989).
28. J. F. Bott and N. Cohen, *Int. J. Chem. Kinet.,* **23,** 1075 (1991).
29. J. Warnatz, in *Combustion chemistry,* W. C. Gardiner, Jr. Ed., Springer-Verlag, New York. 1984, Chap. 5.
30. H. E. Radford, *Chem. Phys. Lett.,* **71,** 195 (1982).
31. G. F. Adams, Eastern States Section Meeting, The Combustion Institute, 1981, p. 9.
32. L. Batt, J. P. Burrows, and G. N. Robinson, *Chem. Phys. Lett.,* **78,** 467 (1981).
33. G. F. Adams, R. J. Bartlett, and G. D. Purvis, *Chem. Phys. Lett.,* **87,** 311 (1982).
34. D. Gutman, N. Sanders, and J. E. Butler, *J. Phys. Chem.,* **86,** 66 (1982).

35. H.-J. Spangenberg, J. Lachmann, I. Börger, L. Dessau, W. Fiebig, and A. A. Levitsky, *Z. Phys. Chem.,* **271,** 5 (1990).
36. W. Tsang and R. F. Hampson, *J. Phys. Chem. Ref. Data,* **15,** 1087 (1986).
37. R. J. Kee, F. M. Rupley, and J. A. Miller, *The Chemkin thermodynamic data base.* SAND87-8215B, Sandia National Laboratories, Livermore, CA (1987).
38. J. A. Seetula and D. Gutman, *J. Phys. Chem.,* **96,** 5401 (1992).
39. R. J. Kee, F. M. Rupley, and J. A. Miller, *Chemkin-II: A Fortran chemical kinetics package for the analysis of gas-phase chemical kinetics.* SAND89-8009, Sandia National Laboratories, Livermore, CA (1989).
40. A. E. Lutz, R. J. Kee, and J. A. Miller, *SENKIN: A Fortran program for predicting homogeneous gas phase chemical kinetics with sensitivity analysis.* SAND87-8248, Sandia National Laboratories, Livermore, CA (1987).
41. R. Fort and C. N. Hinshelwood, *Proc. Roy. Soc. London A,* **129,** 284 (1930).
42. W. A. Bone and J. B. Gardner, *Proc. Roy. Soc. London A,* **154,** 297 (1936).
43. K. M. Bell and C. F. H. Tipper, *Proc. Roy. Soc. London A,* **238,** 256 (1956).
44. M. Cathonnet, J. C. Boettner, and H. James, *J. Chim. Phys.,* **79,** 475 (1982).
45. K. W. Aniolek and R. D. Wilk, *Energy & Fuels,* **9,** 395 (1995).
46. K. M. Bell and C. F. H. Tipper, *Trans. Faraday Soc.,* **53,** 982 (1957).
47. E. J. Harris, *Trans. Faraday Soc.,* **44,** 764 (1948).
48. D. Aronowitz, R. J. Santoro, F. L. Dryer, and I. Glassman, *17th Symp. (Int.) Combust.,* 633 (1979).
49. D. F. Cooke, M. G. Dodson, and A. Williams, *Combust. Flame,* **16,** 233 (1971).
50. T. Tsuboi and K. Hashimoto, *Combust. Flame,* **42,** 61 (1981).
51. P. H. Cribb, J. E. Dove, and S. Yamazaki, *Combust. Flame,* **88,** 186 (1992).
52. H. Hippler, H. Neunaber, and J. Troe, *J. Chem. Phys.,* **103,** 3510 (1995).
53. W. H. Wiser and G. R. Hill, *5th Symp. (Int.) Combust.,* 553 (1955).
54. G. J. Gibbs and H. F. Calcote, *J. Chem. Eng. Data,* **4,** 226 (1959).
55. M. Hirano, K. Oda, T. Hirano, and K. Akita, *Combust. Flame,* **40,** 341 (1981).
56. M. Metghalchi and J. C. Keck, *Combust. Flame,* **48,** 191 (1982).
57. R. Akrich, C. Vovelle, and R. Delbourgo, *Combust. Flame,* **32,** 171 (1978).
58. L. L. Andersson, B. Christenson, A. Hoglund, J. O. Olsson, and L. G. Rosengren, *Prog. Astro. Aero.,* **95,** 164 (1984).
59. J. O. Olsson, L. S. Karlsson, and L. L. Andersson, *J. Phys. Chem.,* **90,** 1458 (1986).
60. J.-F. Pauwels, M. Carlier, and L.-R. Sochet, *J. Phys. Chem.,* **86,** 4330 (1982).
61. C. K. Westbrook and F. L. Dryer, *Combust. Flame,* **37,** 171 (1980).
62. J. E. Dove and J. Warnatz, *Ber. Bunsenges. Phys. Chem.,* **87,** 1040 (1983).
63. J. O. Olsson, I. B. M. Olsson, and L. L. Andersson, *J. Phys. Chem.,* **91,** 4160 (1987).
64. C. M. Vagelopoulos, F. N. Egolfopoulos, and C. K. Law, *25th Symp. (Int.) Combust.,* 1341 (1994).
65. K. Hoyermann, N. S. Loftfield, R. Sievert, and H. G. Wagner, *18th Symp. (Int.) Combust.,* 831 (1981).
66. P. Heinemann-Fiedler and K. Hoyermann, *Ber. Bunsenges. Phys. Chem.,* **92,** 1472 (1988).
67. P. Roth and T. Just, *20th Symp. (Int.) Combust.,* 807 (1984).
68. A. J. Marchese and F. L. Dryer, *Combust. Flame,* **105,** 104 (1996).
69. A. J. Marchese, F. L. Dryer, M. V. Nayagam, and R. Colantonio, *26th Symp (Int.) Combust.,* 1209 (1997).
70. A. J. Marchese, F. L. Dryer, M. V. Nayagam, and R. Colantonio, *26th Symp (Int.) Combust.,* 1219 (1997).
71. A. J. Marchese and F. L. Dryer, *Combust. Sci. and Tech.,* **124,** 373 (1997).
72. A. J. Marchese, R. O. Colantonio and F. L. Dryer), *Radiative Effects in Space-Based Methanol/Water Droplet Combustion Experiments,* 27th Symp. (Int)Combust. (1998). (In press.)
73. D. Lee, S. Hochgreb, and J. C. Keck, *Autoignition of alcohols and ethers in a rapid compression machine,* SAE Paper 932755 (1993).
74. A. N. Pirraglia, J. V. Michael, J. W. Sutherland, and R. B. Klemm, *J. Phys. Chem.,* **93,** 282 (1989).
75. J. W. Sutherland, J. V. Michael, A. N. Pirraglia, F. L. Nesbitt, and R. B. Klemm, *21st Symp. (Int.) Combust.,* 929 (1986).
76. J. V. Michael and J. W. Sutherland, *J. Phys. Chem.,* **92,** 3853 (1988).
77. J. W. Sutherland, P. M. Patterson, and R. B. Klemm, *23th Symp. (Int.) Combust.,* 51 (1990).
78. N. Cohen and K. R. Westberg, *J. Phys. Chem. Ref. Data,* **12,** 531 (1983).
79. R. F. Hampson, *Chemical kinetic and photochemical data sheets for atmospheric reactions.* FAA-EE-80-17, U.S. Dept. of Transportation, FAA, Washington, DC (1980).
80. D. L. Baulch, D. D. Drysdale, D. E. Horne, and A. C. Lloyd, "Homogeneous gas phase reactions of the H_2—O_2 system," In *Evaluated kinetic data for high temperature reactions,* London, Butterworths, 1972.
81. C. J. Cobos, H. Hippler, and J. Troe, *J. Phys. Chem.,* **89,** 342 (1985).
82. M. W. Slack, *Combust. Flame,* **28,** 241 (1977).
83. D. L. Baulch, R. A. Cox, R. F. Hampson, J. A. Kerr, J. Troe, and R. T. Watson, *J. Phys. Chem. Ref. Data,* **9,** 295 (1980).
84. H. Hippler, J. Troe, and J. Willner, *J. Chem. Phys.,* **93,** 1755 (1990).
85. L. Brouwer, C. J. Cobos, J. Troe, J.-R. Dübal, and F. F. Crimm, *J. Chem. Phys.,* **86,** 6171 (1987).

86. H. Hippler and J. Troe, *Chem. Phys. Lett.*, **192,** 333 (1992).
87. D. L. Baulch, D. D. Drysdale, J. Duxbury, and S. J. Grant, "Homogeneous gas phase reaction of the O_2-O_3 system, the CO-O_2-H_2 systems and of sulphur-containing species," In *Evaluated kinetic data for high temperature reactions*, London, Butterworths, 1976.
88. G. M. Atri, R. R. Baldwin, K. Jackson, and R. W. Walker, *Combust. Flame,* **30,** 1 (1977).
89. R. S. Timonen, E. Ratajczak, D. Gutman, and A. F. Wagner, *J. Phys. Chem.*, **91,** 5325 (1987).
90. R. S. Timonen, E. Ratajczak, and D. Gutman, *J. Phys. Chem.*, **92,** 651 (1988).
91. R. S. Timonen, E. Ratajczak, and D. Gutman, *J. Phys. Chem.*, **91,** 692 (1987).
92. NASA, *Chemical kinetics and photochemical data for use in stratospheric modeling.* JPL Publ. 85-37, NASA Panel for Data Evaluation (1985).
93. R. R. Baldwin, A. R. Fuller, D. Longthorn, and R. W. Walker, *J. Chem. Soc. Faraday I,* **70,** 1257 (1974).
94. M. Page, M. C. Lin, Y. He, and T. K. Choudhury, *J. Phys. Chem.*, **93,** 4404 (1989).
95. C. T. Bowman, R. K. Hanson, D. F. Davidson, W. C. Gardiner, Jr., V. Lissianski, G. P. Smith, D. M. Golden, M. Frenklach, and M. Goldenberg, *GRI-MECH.* (1996).
96. P. J. Wantuck, R. C. Oldenborg, S. L. Baughcum, and K. R. Winn, *J. Phys. Chem.*, **91,** 4653 (1987).
97. E. A. Lissi, G. Massiff, and A. E. Villa, *J. Chem. Soc. Faraday I,* **69,** 346 (1973).
98. I. R. Slagle, D. Sarzynski, and D. Gutman, *J. Phys. Chem.*, **91,** 4375 (1987).
99. I. A. B. Reid, C. Robinson, and D. B. Smith, *22nd Symp. (Int.) Combust.*, 1833 (1988).
100. A. F. Wagner and D. M. Wardlaw, *J. Phys. Chem.*, **92,** 2462 (1988).
101. W. Tsang, *Combust. Flame,* **78,** 71 (1989).
102. G. C. Schatz, A. F. Wagner, and T. H. Dunning Jr. *J. Phys. Chem.*, **88,** 221 (1984).
103. J. W. Sutherland, J. V. Michael, and R. B. Klemm, *J. Phys. Chem.*, **90,** 5941 (1986).
104. W. Felder and S. Madronich, *Combust. Sci. and Tech.*, **50,** 135 (1986).
105. R. W. Walker, *A critical survey of rate constants for reactions in gas-phase hydrocarbon oxidation,* Burlington House, London, 1975.
106. K. Saito, T. Kakumoto, H. Kuroda, S. Torii, and A. Imamura, *J. Chem. Phys.*, **80,** 4989 (1984).
107. G. S. Jolly, D. J. McKenney, D. L. Singleton, G. Paraskevopoulos, and A. R. Bossard, *J. Phys. Chem.*, **90,** 6557 (1986).
108. H. H. Grotheer, G. Riekert, D. Walter, and T. Just, *J. Phys. Chem.*, **92,** 4028 (1988).
109. Thermodynamics Resource Center, *TRC Thermodynamic Tables—Non-hydrocarbons,* The Texas A&M University System, College Station, TX, 1989.